

# Time-Aware Policy Learning for Adaptive and Punctual Robot Control

Yinsen Jia<sup>1</sup>, Boyuan Chen<sup>1,2,3\*</sup>

<sup>1</sup>Department of Electrical and Computer Engineering, Duke University

<sup>2</sup>Department of Mechanical Engineering and Materials Science, Duke University

<sup>3</sup>Department of Computer Science, Duke University

\*To whom correspondence should be addressed; Email: boyuan.chen@duke.edu.

**Temporal awareness underlies intelligent behavior in both animals and humans, guiding how actions are sequenced, paced, and adapted to changing goals and environments. Yet most robot learning algorithms remain blind to time. We introduce time-aware policy learning, a reinforcement learning framework that enables robots to explicitly perceive and reason with time as a first-class variable. The framework augments conventional reinforcement policies with two complementary temporal signals, the remaining time and a time ratio, which allow a single policy to modulate its behavior continuously from rapid and dynamic to cautious and precise execution. By jointly optimizing punctuality and stability, the robot learns to balance efficiency, robustness, resiliency, and punctuality without re-training or reward adjustment. Across diverse manipulation domains from long-horizon pick and place, to granular-media pouring, articulated-object handling, and multi-agent object delivery, the time-aware policy produces adaptive behaviors that outperform standard reinforcement learning baselines by up to 48% in efficiency, 8 times more robust in sim-to-real transfer, and 90% in acoustic quietness while maintaining near-perfect success rates. Explicit temporal**

**reasoning further enables real-time human-in-the-loop control and multi-agent coordination, allowing robots to recover from disturbances, re-synchronize after delays, and align motion tempo with human intent. By treating time not as a constraint but as a controllable dimension of behavior, time-aware policy learning provides a unified foundation for efficient, robust, resilient, and human-aligned robot autonomy.**

## Introduction

Time is among the most fundamental dimensions of intelligent behavior (1, 2, 3). Humans instinctively adjust how fast or slow they move (4): hurrying when seconds matter, slowing down to ensure precision, or synchronizing seamlessly with others under shared schedules. The awareness of time is a central element of cognition that shapes how to perceive, decide, and collaborate.

Despite major progress in robot learning, most robot policies remain blind to time (5, 6, 7). Current methods typically optimize for task success or accumulated rewards, without explicit mechanisms to allocate or adapt behavior under time awareness. Consequently, robots that achieve a high task success rate can still behave unpredictably or inefficiently both in simulation and the real world, and they lack the controllability with respect to time that human users and partners require. Severe gaps remain when robots operate in dynamic (8, 9), collaborative (10), or safety-critical environments (11, 12).

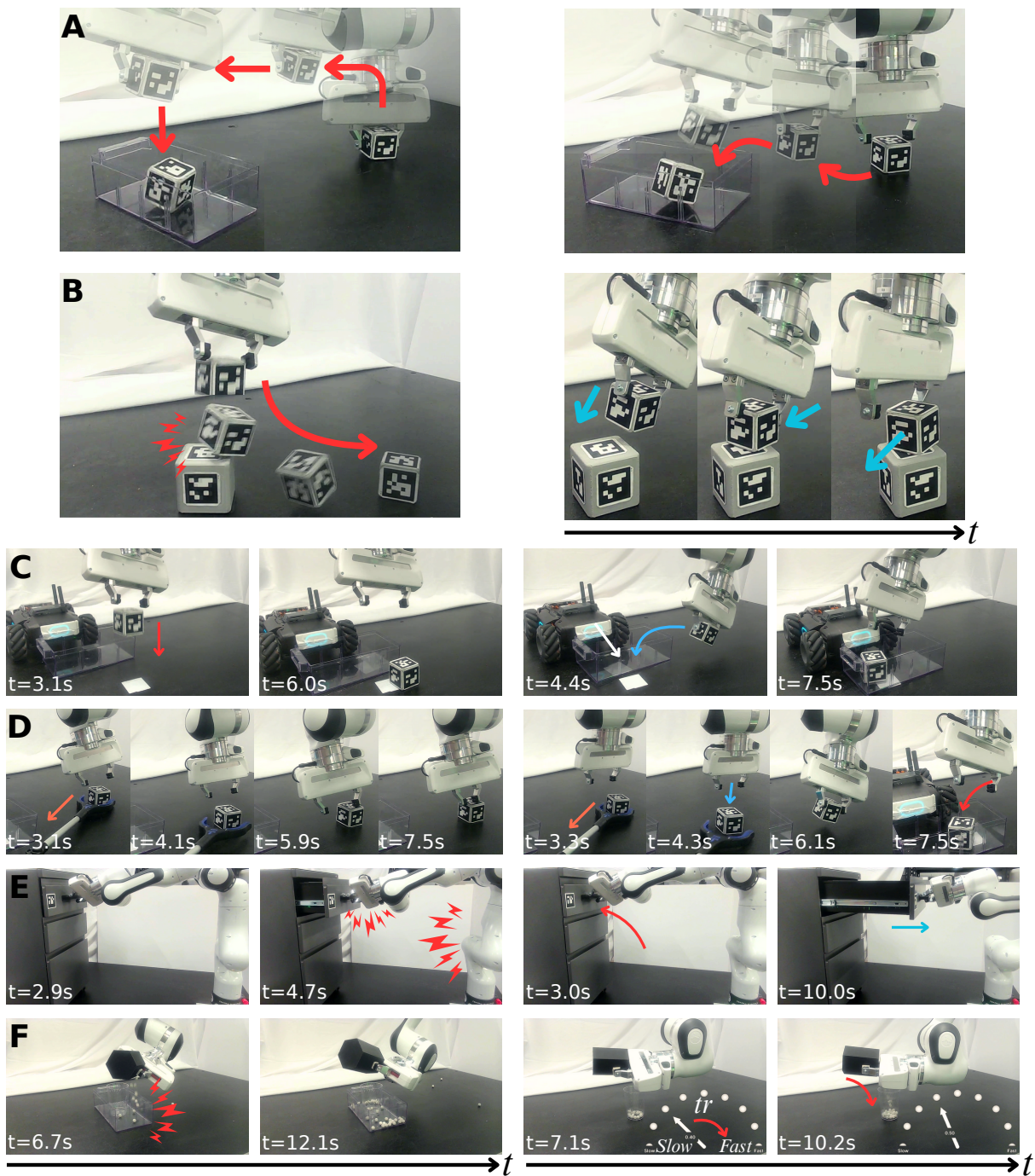
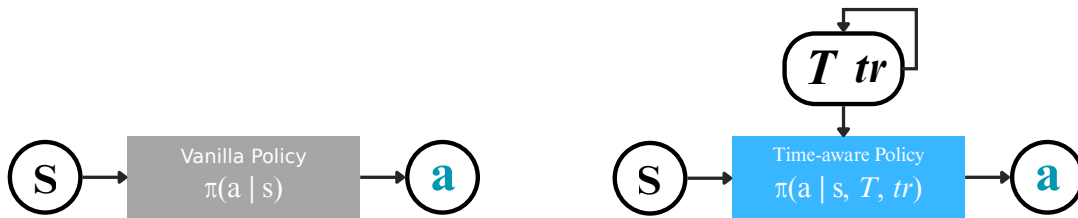
Making robots time-aware is therefore essential. Nearly all forms of robot interactions hinge on how actions unfold in time. In manipulation, effective use of time enables adaptive phase transitions: moving rapidly across free space for task efficiency while slowing down to stabilize contact-rich interactions such as grasping, stacking, pouring, or navigating through cluttered scenes. In human-robot or multi-robot collaboration, timing becomes the “glue” that binds agents together. Being aware of time will allow one partner to anticipate the completion or temporal requirements of others, hence coordinate without collisions or delays. In deployments, flexible use of time can absorb the cost introduced by disturbances or simulation-to-reality (sim2real) mismatches, reducing the need for costly re-training. Beyond reliability, explicit temporal control can offer a new form of user interface: a way to steer robots toward aggressive or cautious behaviors depending on context

and preference. Without explicit reasoning about time, these capabilities remain out of reach with existing approaches.

Enabling time awareness in policy learning is not straightforward. Conventional reinforcement learning (RL) focuses on maximizing cumulative reward (13, 14, 15, 16, 17), which often overlooks explicit awareness of time. The learned policies may appear successful by task success metrics, but often produce undesirable artifacts through reward hacking, such as stalling or idling at certain stages and then rushing abruptly to meet terminal conditions (18, 19, 20, 21). These behaviors are brittle to changes in the environment, transfer poorly to the real world, and provide little flexibility for collaborations with humans or other robots without extensive re-training.

To further illustrate the challenging nature of this problem, let us consider a small subset of the task: slowing down the task execution from a faster policy. A straightforward solution is to interpolate the fast motions into slower ones. However, this method easily fails. First, slow motions obtained through interpolation do not guarantee robustness in contact-rich tasks, where instability arises from object dynamics rather than motion speed. To handle objects in a more robust way, though it appears that the motion should be “slower”, the behavior may require more nuanced changes. For example, pouring a larger number of beans into a container requires much more fine-grained manipulation skills than simply being slower than pouring a few beans. Second, interpolated motions sacrifice responsiveness, leaving the robot unable to adapt to environmental changes such as disturbances. Finally, timing still remains unpredictable and unadaptable since there is no inherent motivation for the policy to follow variable scheduled time. Movie S2, Movie S5, and Movie S6 emphasize these subtle but critical differences.

While prior research has explored temporal awareness in robotics, time has largely been treated as an auxiliary parameter rather than an explicit and controllable factor in behavior generation. Early temporal scheduling frameworks in collaborative robotics (22) emphasize synchronization and robustness under human-defined timing constraints but do not integrate temporal reasoning into the control policy itself. Similarly, studies in human-robot interaction (23, 24) have examined when a robot should act to maintain fluency, relying on pre-specified synchronization cues rather than learning how to adapt action timing to task dynamics. In learning-based robotics, time is typically used for reward discounting or state regularization. Agents incorporate time as an observation that affects value estimation but not as a variable that shapes their motion or phase progression (25, 26).



Other works have utilized temporal signals to offset communication delays, manage execution order, or compensate for latency (27, 28, 29, 30, 31, 32). However, these approaches primarily correct for timing errors rather than leveraging time to structure control behavior. Even in multi-agent and planning domains, where timing is central to coordination (33, 34, 35, 36, 37), methods typically depend on predefined schedules or task-specific heuristics. Overall, existing work focuses on compensating for time rather than leveraging it as an explicit variable that shapes the evolution and adaptation of robot behaviors.

Our central hypothesis is that if time is explicitly integrated into policy learning, not only as an observation as in previous studies, but also as a controllable signal to shape intrinsic behaviors, then robots will not only complete tasks within scheduled time, but also naturally discover dynamic skills, adaptive strategies, punctual coordination, and controllable modes of operation that are otherwise inaccessible. In this view, time is more than a constraint. Time becomes a universal driver for emergent capabilities: efficiency through the discovery of fast dynamics (e.g., sliding, throwing), stability through purposeful use of surplus time, punctuality through adherence to deadlines, and robustness through flexible temporal reallocation when disturbances arise.

In this paper, by building on the above hypothesis, we introduce Time-Aware Policy Learning

---

**Figure 1** (*preceding page*): **Time-aware policy enables adaptive, punctual, robust, and controllable manipulation behaviors.** Unlike a standard policy  $\pi(a | s)$ , which lacks temporal context, a time-aware policy  $\pi(a | s, T, tr)$  conditions actions on remaining time  $T$  and a time-ratio command  $tr$  to control internal perception of time inside the robot’s policy. **(A)** Under tight time constraints, the time-aware policy adopts dynamic strategies (e.g., sliding, throwing) that achieve higher manipulation efficiency than the vanilla policy. **(B)** When more time is available, the policy exhibits careful and stable behaviors that reduce the sim-to-real gap, adapt to environment changes, and reduce manipulation noise. **(C)** Predictable manipulation timing enables punctual, adaptive responses that facilitate multi-agent collaboration. **(D)** Following unexpected perturbations, time-aware policy re-establishes contact and then accelerates to meet the deadline. **(E)** Stage-wise temporal modulation produces fast approach and transport, followed by deliberate grasping and placement without retraining. **(F)** Real-time user control of  $tr$  allows on-the-fly adjustment between cautious and aggressive modes, enabling correction under unmodeled dynamics and unseen disturbances.

(Fig. 1), a unified reinforcement learning framework that endows robot policies with explicit time awareness. Time-aware policy incorporates two complementary signals into policy training: the remaining time, which specifies how much time the robot has left to complete the task, and a time ratio, which determines the speed of the robot’s internal perception of time elapses. By conditioning actions on these signals, the resulting policy can not only meet the scheduled time but also flexibly adjust its behavior in real time, trading speed for stability as required by the task or user. For example, under tight budgets, the policy naturally discovers dynamic strategies such as sliding, swinging, or throwing to minimize task duration, while with surplus time, it adopts cautious, deliberate movements to stabilize contact-rich interactions and improve success rates.

Once trained, a single time-aware policy can be reused across diverse settings without re-training. The time ratio functions as a simple and intuitive “dial”, allowing users or higher-level planners to modulate robot behavior online, from aggressive to careful, without modifying low-level parameters. This controllability is particularly valuable in collaborative contexts, where predictable timing enables seamless coordination with humans or other robots. Moreover, the same policy can adapt to environmental disturbances or simulation-to-reality mismatches by reallocating its scheduled time on the fly, thereby reducing the need for exhaustive domain randomization. By elevating time to a first-class learning signal, our work turns time-aware robot policy learning into a foundation for efficiency, stability, robustness, and intuitive human control. See Movie S1 for the overview of the motivation, key idea, and demonstrations.

In the following sections, we begin by describing our main methods (Fig. 2) for constructing time-aware robot policies. We then follow up with experimental results and evaluations to demonstrate how the learned policy can benefit robot deployments in various tasks and settings.

### **Learning the temporal lower bound**

To make policy learning time-aware, the robot needs to first understand what constitutes an efficient use of time. We therefore begin by estimating the temporal lower bound that describes the minimum duration in which a task can be feasibly completed. This lower bound not only quantifies the intrinsic efficiency limit of the robot itself, but also establishes a reference scale for later adaptation where slower behaviors can be shaped as deliberate deviations from this efficient baseline rather than unstructured delays.

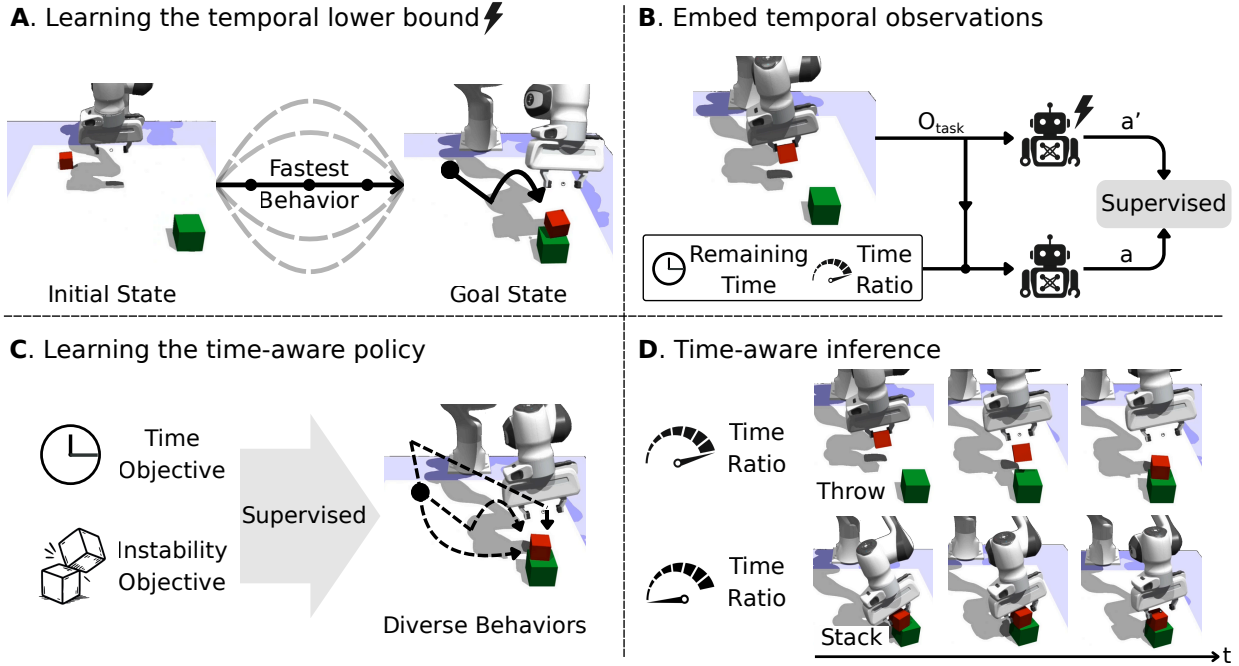


**Figure 2: Time-aware policy learning pipeline.** (A) A standard RL policy is first refined with a minimum-time objective to obtain the fastest feasible strategy, producing a temporal lower bound and an empirical upper bound on instability. (B) Remaining time  $T^{\text{left}}$  and time-ratio  $tr$  signals are then appended to the observation space, and the time-optimal policy is distilled into this augmented policy via behavior cloning to preserve high-speed behaviors. (C) The augmented policy is further trained with a time objective and an instability constraint, enabling adaptive execution across schedules while ensuring effective usage of the available time. (D) At inference, varying  $tr$  modulates action tempo: larger  $tr$  induces fast, momentum-exploiting behavior (e.g., throw-like placement), while smaller  $tr$  yields slow, precise motions (e.g., careful stacking) without retraining.

We consider the decision-making problem as a Markov Decision Process (MDP) with objective:

$$J_R(\pi) = \mathbb{E} \left[ \sum_{t=0}^{\infty} \gamma^t r(s_t, a_t, s_{t+1}) \right], \quad (1)$$

where  $s_t$  and  $a_t$  denote the current state and action,  $r(\cdot)$  is the reward function,  $\gamma$  is the discount factor ( $0 \leq \gamma \leq 1$ ), and  $\pi$  represents the robot policy. Typically, the policy is trained to maximize expected total returns as in Eq. 1 through reinforcement learning. For challenging tasks, the reward function  $r(\cdot)$  typically involves a dense reward component to guide the learning and a large terminal reward for final task success.

Yet, a vanilla policy trained under this conventional formulation optimizes task success but is not necessarily time-optimal (25). Consequently, even successful trajectories often contain idle or redundant actions that waste time or energy, as widely observed in practice.

Retrieving a time-optimal policy, though seemingly straightforward, is in fact a challenging problem that has rarely been visited before. If a policy is trained to complete a task as soon as possible while learning how to do so, it can struggle to converge due to the challenging optimization problem. It becomes more difficult when the task itself requires complex skills and long horizons. Therefore, we adopt a two-stage strategy. First, we train a vanilla policy using Eq. 1 so that the policy learns to complete the task with a high success rate. Then, we continue the policy training to emphasize efficiency.

A naive method is to continue the training with only a terminal success reward:

$$J_R(\pi) = \mathbb{E} \left[ \mathbb{1}_{\text{success}} \cdot \gamma^t R \right], \quad (2)$$

where  $\mathbb{1}_{\text{success}}$  indicates task success. Under this setting, in order to achieve a high return, the policy must learn to complete the task as fast as possible. However, this formulation is highly sensitive to the choice of  $\gamma$  (38). When  $\gamma$  is small, reward signals at earlier steps will vanish, especially in long-horizon tasks, which is known as reward vanishing problem. Therefore, a common choice of  $\gamma$  is a large value that is close to 1 (e.g., 0.995). However, recent work (25) has shown that, when  $\gamma$  is close to 1, the policy cannot properly capture the advantage differences across trajectories of varying lengths, which prevents the agent from prioritizing efficiency and may lead to return aliasing and training instability.

We mitigate this trade-off by preserving a large  $\gamma$  while augmenting the terminal reward with the remaining time  $T_N^{\text{left}}$  at completion:

$$J_R(\pi) = \mathbb{E} \left[ \mathbb{1}_{\text{success}} \cdot \gamma^t (R \cdot T_N^{\text{left}}) \right], \quad (3)$$

where  $N$  is the maximum allowed episode length. This simple modification provides a well-behaved gradient signal that directly favors more efficient trajectories. Intuitively, trajectories that complete with greater remaining time receive proportionally higher rewards, explicitly aligning policy optimization with temporal efficiency.

The resulting time-optimal policy naturally discovers dynamic behaviors, such as sliding, swinging, or throwing, to exploit physical dynamics to shorten task duration. By executing this policy across diverse randomized environments, we record the average minimum completion time  $t^{\min}$ , which serves as the temporal lower bound for the corresponding task configuration. This value defines the feasible time window for all subsequent stages of training, so the behaviors will not be expected to be faster than physically achievable. The temporal lower bound is a meaningful reference for allocating longer or more deliberate behaviors during time-aware policy learning in the following sections.

### Learning the time-aware policy

Once we establish the temporal lower bound, the next step is to make the robot’s policy explicitly aware of time to be able to perceive how much time remains, plan how to use it, and adapt its actions accordingly. Our goal is to train a single unified policy that can operate under various temporal requirements: completing tasks punctually when the available time is short, but acting cautiously and stably when ample time remains. In our framework, time becomes both an observation and a control signal to shape behavior from within the policy itself rather than being imposed externally.

**Define the time-aware punctuality objective.** To ensure that the robot completes a task within a desired schedule while allowing adaptive tempo control, we define a time-aware punctuality objective. Each episode begins with a scheduled duration derived from the previously estimated minimum completion time  $t^{\min}$ . The policy maintains a remaining time variable  $T_t^{\text{left}}$ , which decreases during execution according to a controllable time ratio  $tr$ . This ratio modulates how quickly

the robot perceives time to elapse and, consequently, how aggressively it acts:

$$c^{\text{time}} = \left| \frac{T_N^{\text{left}}}{tr_N} \right|, \quad T_0^{\text{left}} = t^{\text{min}}, \quad T_{t+1}^{\text{left}} = T_t^{\text{left}} - \Delta t \cdot tr. \quad (4)$$

Here,  $c^{\text{time}}$  penalizes the mismatch between the scheduled and actual completion time, encouraging punctual task execution.  $T_N^{\text{left}}$  is the remaining time at the end of the episode,  $T_0^{\text{left}}$  is the scheduled time, and  $\Delta t$  is the real-world time interval. A larger  $tr$  accelerates the perceived passage of time, prompting faster and more dynamic motions, while a smaller  $tr$  slows the perceived clock, encouraging more deliberate and stable behaviors. During training,  $tr$  is fixed within each episode but varied across episodes to expose the policy to different temporal conditions. During deployment, it becomes a real-time control input  $tr_t$ , enabling smooth modulation of the robot’s tempo according to user intent, environmental uncertainty, or coordination needs with other agents.

**Ensuring effective use of time.** Although the temporal conditioning allows controllability, it does not inherently ensure that the available time will be used effectively. Without additional guidance, a robot might still idle for certain period of an episode and act only near the end. In this case, the robot could still achieve punctuality, but its behavior is not desirable. To address this, we introduce a simple but effective stability objective to penalize excessive scene motion. We define a scalar measure of *scene instability* as the sum of the velocities of all movable objects, excluding the robot itself, and constrain it relative to a threshold scaled by  $tr_t$  (Method: Define the instability objective). When more time is available (i.e., small  $tr_t$ ), the policy is encouraged to favor gentle and stable motions. When time is limited (i.e., large  $tr_t$ ), it allows more dynamic interactions to maintain punctuality. This auxiliary constraint helps the robot learn how to spend time effectively without overshadowing the main task and time objective.

The resulting time-aware policy is a unified model that integrates environmental perception with temporal awareness. At each step, the policy receives as input the environment state and two temporal variables ( $s, T_t^{\text{left}}, tr_t$ ), and outputs a continuous action  $a_t$  that satisfies both task goals and temporal requirements. We first train the policy by embedding time-aware observations through behavior cloning from the most efficient policy, ensuring that the introduction of temporal inputs does not degrade its original task performance. During this stage, the robot learns to interpret  $T_t^{\text{left}}$  and  $tr_t$  as contextual cues that influence action timing and intensity, without optimizing for punctuality yet. After convergence, the augmented policy retains the dynamic skills from the

efficient policy while being trained further to obtain the ability to condition behaviors on perceived time. Once trained, the same policy can be deployed under any time ratio, acting swiftly under high urgency or gently when time is abundant, all through a single scalar command. Our compact control structure allows a single model to adapt across task speeds, phases, and collaborative scenarios.

## Results

We evaluate the time-aware policy across simulation and real-world experiments. Our focus is to study how time awareness influences efficiency, stability, punctuality, adaptability, and controllability. Our primary goal is to demonstrate that explicit time awareness enables robots to adapt their behavior fluidly to different temporal constraints and environmental conditions, without any re-training or reward adjustment.

We utilized three representative and challenging manipulation tasks covering rigid-body, granular media, and articulated object interactions. We further validated the performance on a real robot system, evaluated zero-shot sim-to-real transfer, and demonstrated multi-agent collaboration and real-time human-in-the-loop control through temporal modulation.

### Experimental setup

We used a Franka Panda Research 3 arm as the manipulator for all tasks. Object poses were tracked with ArUco markers with an RGB camera. As shown in Fig. S2, observations were first passed through a noise layer (active only during training). The resulting noisy observations were input to the actor, which generated the 6-DoF end-effector relative pose and a binary gripper action in 20 Hz. The relative pose was converted into target joint positions via differential inverse kinematics. These positions were smoothed with an exponential moving average (EMA) filter and sent to the low-level joint impedance (JI) controller to command the robot arm at a 1 kHz. We estimated the minimum required time for each real-world configuration by querying the five most similar simulation setup and averaging their successful completion time. All evaluations were repeated across at least ten real-robot trials and 2000 randomized simulation configurations per condition.

## Metrics

To quantitatively evaluate the time-aware policy, we use the following metrics:

- **Success rate (%)**: The fraction of trials in which the task is completed successfully.
- **Elapsed time (s)**: The total elapsed time to complete an episode.
- **Time mismatch (s)**: The absolute difference between the scheduled time and the actual elapsed time in successful episodes.
- **Instability (m/s)**: The cumulative object-velocity norm in successful episodes.
- **Maximum acoustic noise (amplitude ratio)**: The maximum acoustic noise level measured during real-world manipulation. This metric is only used in real-world experiments and is computed as  $r_A = \frac{A}{A_{max}}$ , where  $A_{max}$  is the maximum recordable amplitude.

## Tasks

Our tasks are representative examples to evaluate time-aware policy and demonstrate its performance. We expect that our framework can generalize to other related tasks. We chose the following tasks since they capture core challenges of real-world manipulation that require temporal precision, stability under contact, dynamic adaptation, and coordination across agents. They are also often used as benchmarks for assessing generalizable robot control (18, 39, 40).

**Cube placing and stacking.** This task is an instance of classical pick-and-place manipulation. In real-world setting, we used two variants. In cube placing, the robot needs to pick up a cube at a random pose and place it into a box positioned at a random location. In cube stacking, the robot must stack one cube atop another, which demands more fine-grained motion control and alignment under contact. Both variants are deemed as long-horizon tasks which requires multiple steps to complete. An episode succeeds when the cube is placed into the box, or stably stacked on the target cube, while the end-effector is at least 5 cm away from the source cube. Failure will occur if a contact force above 20 N happens with the table or the maximum episode time is reached. We only trained cube stacking in simulation and evaluated both variants in the real world.

**Granular media pouring.** This task assess manipulation with high contact dynamics, where

success depends on controlling many-body interactions. The task requires adaptive temporal modulation and continuous correction based on flow feedback. In real-world setting, we used two variants similar to the above task. The first variant asks the robot to pour the granular particles into a large box while the second variant asks the robot to pour into a small cup. We only trained with a single granular particle in simulation. During testing, we scaled the number of grains up to 40 to evaluate generalization to unseen dynamic complexity. An episode succeeds when all particles are poured into the target container. Failure occurs if any particle is missed out, the grasped cup falls down, a force greater than 20 N is detected on the table, or the maximum episode time is reached. An additional failure condition was used for the second variant to prevent the target cub falls.

**Drawer opening.** This task involves articulated-object manipulation. The robot is tasked to grasp a drawer handle and pull it open to a target displacement of 35 cm. The task requires managing both contact stability and compliant impedance control. These requirements are especially time sensitive because premature or overly rapid pulling can cause slippage or destabilize the grasp. At the start of each episode, a cabinet will be placed in front of the arm with a random 3-DOF translation, and the arm will be initialized in a random joint configuration. Failure occurs if any cabinet component experiences a force greater than 20 N or if the maximum episode time is reached.

**Multi-agent object delivery** This collaborative task evaluates temporal coordination between agents where timing is as critical as physical interaction. A robotic arm and a mobile vehicle are tasked to jointly deliver an object. The vehicle will approach a target location, pause at the meeting location, and then drive back to the final location. The arm must synchronize its placing motion with the vehicle’s arrival time while maintaining stability to deliver the object. The episode succeeds if the object is delivered precisely within the schedule time window.

### **Time awareness improves efficiency and punctuality**

Explicit time awareness substantially enhances both task efficiency and temporal precision. Under the minimum scheduled time ( $tr_t = 1.0$ ), the time-aware policy completed manipulation tasks 18–48% faster than the vanilla RL baseline across all three real-world evaluations (Table 1). In cube placing, granular media pouring, and drawer opening, the time-aware policy adopted dynamic and agile strategies that minimized redundant motion. These behaviors emerged solely from the time objective without any skill-specific rewards. See Movie S3 for more qualitative demonstrations.

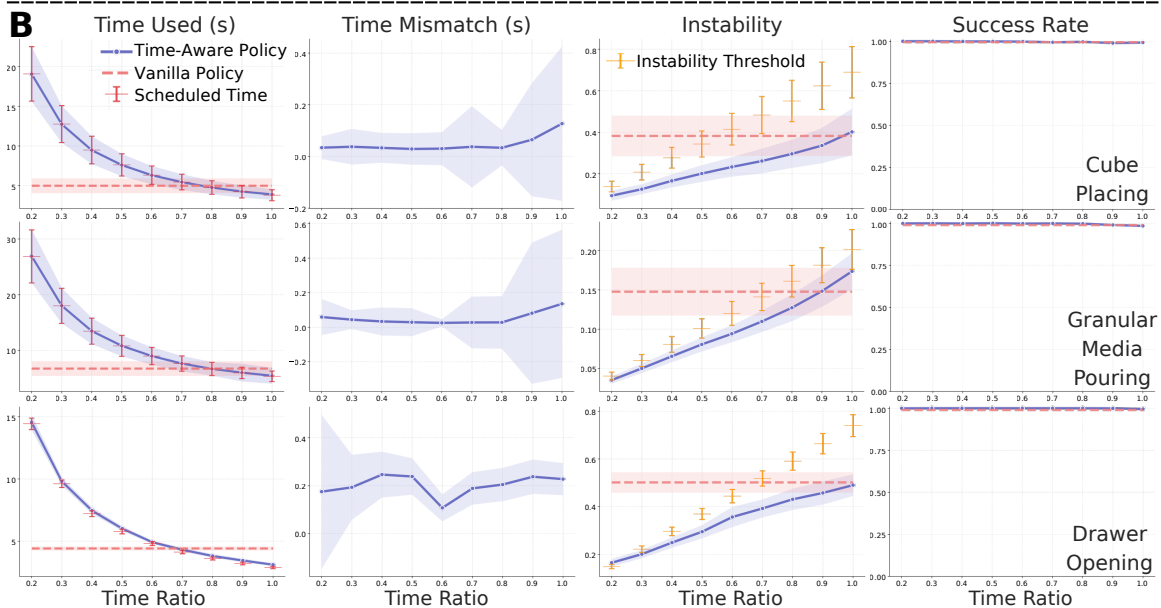
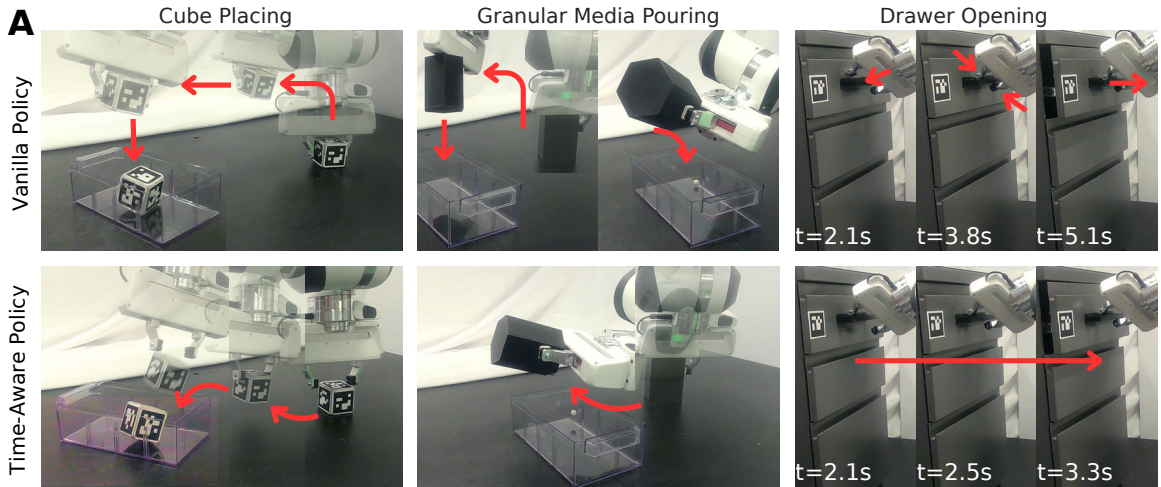


**Figure 3: Time awareness improves efficiency and punctuality.** (A) Real-world execution for three tasks. The vanilla policy performs sequential motions (approach-grasp-lift-place), whereas the time-aware policy leverages momentum and parallelizes phases (e.g., slide-while-grasp, swing-to-pour, and pre-tensioned drawer pull). (B) Simulation benchmarks across time ratio settings. Time used: completion time decreases as the time ratio increases, with the time-aware policy completing tasks faster than the vanilla baseline while adhering to scheduled durations. Time mismatch: the time-aware policy tightly tracks target timing with small completion-time mismatch. Instability: instability increases only when the time ratio is high (fast), remaining below the learned stability threshold when more time is available. Success rate: time-aware policy remain near 100% across tasks and schedules. Explicit temporal conditioning enables aggressive strategies when time is limited and cautious, stable behavior when time is abundant.

**Table 1: Vanilla Policy V.S. Time-aware Policy (Minimum Scheduled Time).** We compared the time used by the vanilla policy and the time-aware policy for different tasks under a minimum scheduled time for 10 successful trials with varying environment configurations in the real world.

Task Name	Vanilla Policy Used Time (s) ↓	Time-aware Policy Used Time (s) ↓
Cube Placing	6.24 ± 0.53	<b>3.25 ± 0.23</b>
Granular Media Pouring (Box)	6.34 ± 0.71	<b>4.21 ± 0.57</b>
Drawer Opening	8.53 ± 0.14	<b>7.03 ± 0.48</b>

As shown in Fig. 3(A), in cube placing, unlike the vanilla RL policy that took a strategy to approach, grasp, lift, align, and then release the cube, the time-aware policy performed multiple actions in parallel. The robot learned to slid while grasping, and lifted while transporting, leveraging object inertia to execute throw-like motions into the container. In granular media pouring, the time-aware policy initiated flow by swinging the cup during transport to shorten the pouring time. In drawer opening, the time-aware policy simultaneously closed the gripper and began pulling in order to eliminate idle waiting after contact. All of these dynamic behaviors were learned in simulation with explicit time awareness and directly transferred zero-shot to the real robot.

Our large-scale simulation evaluations with 2000 random configurations per task and time ratio further confirmed these trends (Fig. 3(B)). While the vanilla RL baseline remained static behaviors without any adaptation abilities to different time schedules, the time-aware policy strictly adhered to schedule time with an average mismatch below 0.6 s across all time ratios. When the time ratio was set to 1, the time-aware policy used 25% less time, while maintaining the original success rate (> 99%). When the time ratio decreases, the time-aware policy effectively used the additional time to act cautiously, ensuring the instability stays below the designated threshold.

### **Adaptive stability and environmental robustness**

We next examined whether time awareness improves generalization and stability under environment changes that were not seen during training. We modified the real-world tasks to require more delicate operations for task success. Using the same three task families, we introduced modifications that

**Table 2: Vanilla Policy V.S. Time-aware Policy ( $2\times$  Minimum Scheduled Time).** We compared the performance between the vanilla policy and the time-aware policy under  $2 \times t^{\min}$  scheduled time for 10 trials with varying environment configurations in the real world.

Task Name	Vanilla Policy		Time-aware Policy	
	Success Trials $\uparrow$	Max Noise $\frac{A}{A_{max}} \downarrow$	Success Trials $\uparrow$	Max Noise $\frac{A}{A_{max}} \downarrow$
Cube Stacking	1/10	$1.0 \pm 0.0$	<b>9/10</b>	<b><math>0.09 \pm 0.04</math></b>
Pouring (40)	0/10	$1.0 \pm 0.0$	<b>8/10</b>	<b><math>0.73 \pm 0.15</math></b>
Drawer Opening	6/10	$0.53 \pm 0.14$	<b>10/10</b>	<b><math>0.03 \pm 0.01</math></b>

created substantial mismatches between training and deployment conditions. Specifically, in the cube placing task, we replaced the box container with another small cube to form the cube stacking task. In the granular media pouring task, we replaced the box container with a same-size cup and increased the number of granular particles from 1 to 40. All the training process used only 1 particle. In the drawer opening task, we added 2 kg of additional weight to the drawer to simulate heavier and unseen loads. These changes altered object dynamics, contact friction, and actuator impedance, which introduce large-sim-to-real discrepancies.

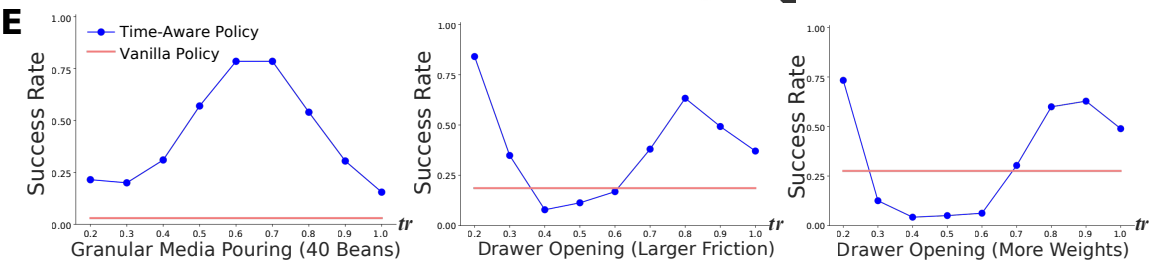
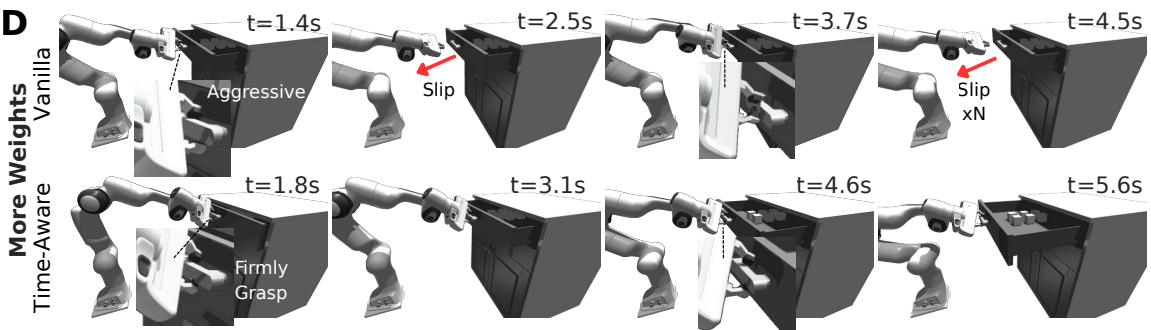
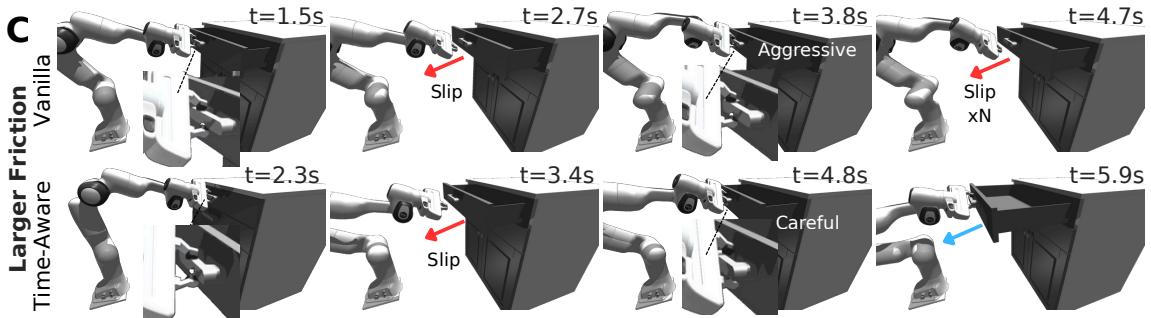
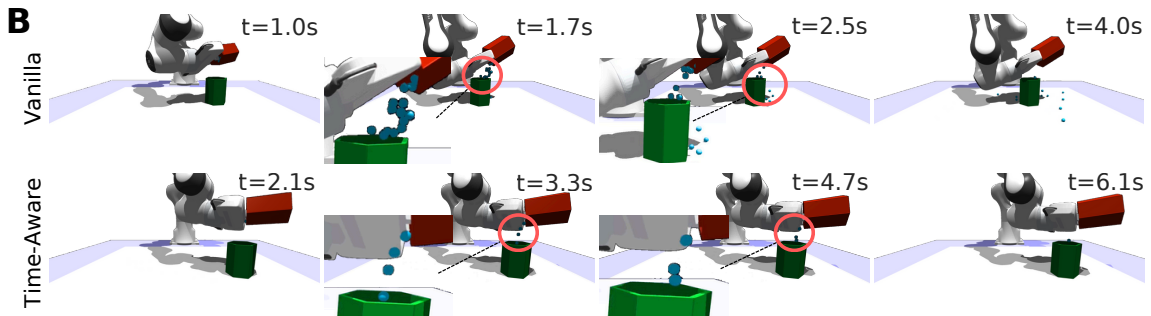
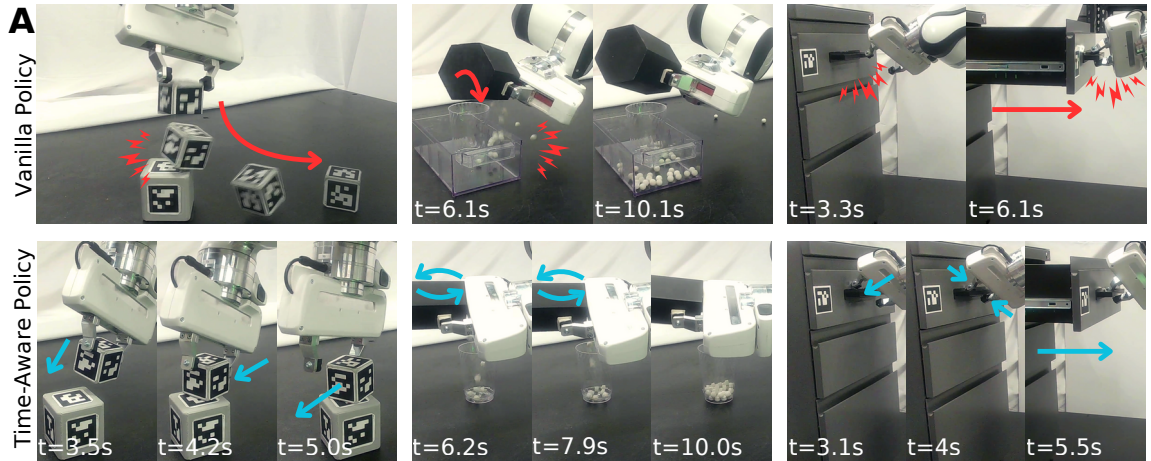
Under these modifications, the vanilla RL policy degraded significantly across all tasks. Fig. 4(A) illustrates the representative failure modes. In the cube stacking task, the vanilla policy consistently failed to align cubes due to unmodeled friction and material properties, revealing a clear sim-to-real dynamics mismatch. In granular pouring, it exhibited a strong bias toward its training experience: despite the larger number of particles, it maintained aggressive pouring motions that caused severe spillage. In the drawer opening, the vanilla policy often pulled too rapidly. Increasing the weight in the drawer creates a persistent lag between commanded and actual joint positions. This accumulated lag further destabilized the impedance of control due to the large torque requirements.

Traditionally, adapting to such environment shifts would require costly real-to-sim remapping to re-register physical properties, followed by policy fine-tuning. This process is not only labor-intensive but also brittle. Any further change in dynamics or inaccurate identification in the last loop may require another round of simulation calibration and retraining.

In contrast, we found that we could adapt time-aware policy to all modified conditions simply by increasing the scheduled time. By doubling the scheduled time, the time-aware policy immediately mitigated all observed issues without any re-training or reward adjustment. As shown in Fig. 4(A) and summarized in Table 2, the time-aware policy demonstrated strong stability and adaptation across all tasks. In cube stacking, the time-aware policy carefully aligned the top cube with the bottom cube. It reduced contact instability and achieved a 9/10 success rate compared with only 1/10 for the vanilla RL policy. In granular pouring, the time-aware policy executed a stable and sequential pouring sequence and achieved 8/10 success in this new high-complexity setting, even showing emergent motions of gentle shaking to release residual beans. In drawer opening, allocating more time enabled the policy to firmly grasp the handle and gradually increase pulling force. These behaviors effectively eliminated lag and stabilized the impedance control loop.

Moreover, a major but underexplored challenge in daily life robotic manipulation is that careless behaviors, such as dropping or hitting objects can generate excessive noise. Reducing manipulation noise through reward tuning and sensor measurement feedback is often costly. As shown in Table 2, the maximum acoustic noise during these manipulations done by the time-aware policy dropped by over 90% compared with the baseline. Moreover, when provided with more time, the motions became even quieter, which is essential for household applications where humans are present. See Movie S4 for more qualitative demonstrations.

To further quantify adaptation at scale, we performed similar experiments in simulation with 2000 randomized configurations for each task and time ratio. For cube stacking, we increased the restitution coefficients of both cubes from 0.1 to 0.5 to approximate the higher bounciness observed in real-world materials. The results closely mirrored the physical experiments. The vanilla RL policy achieved only a 15.3% success rate, whereas the time-aware policy maintained a 99.2% success rate by doubling the schedule time. In granular pouring (Fig. 4(B)), the vanilla policy remained overly aggressive, spilling many grains as the cup filled. The time-aware policy, by contrast, automatically adjusted its strategy according to the time ratio. Providing slightly more time led to cautious and low-velocity pouring that ensured success, whereas excessively conservative ratios prevented some grains from leaving the cup. The best performance occurred at intermediate time ratios. Overly slow motions can be as suboptimal as overly fast ones, emphasizing the necessities of explicit time-awareness in robot policies.



For the drawer-opening task, we examined two additional perturbations that often occur in deployment. First, we increased the cabinet’s joint friction to simulate unmodeled resistance. The vanilla policy repeatedly slipped during grasp due to its aggressive pulling, which leads to repeated failures (Fig. 4(C) and Movie S5). In contrast, the time-policy effectively used the additional given time to adapt its pulling behavior by maintaining firm grasp force and slower extension, and even recovered reliably after minor slips (Movie S5). Interestingly, intermediate time ratios of 0.3 – 0.7 yielded the lowest performance, unlike in the granular pouring task, suggesting that each manipulation domain possesses distinct optimal temporal strategies.

Second, we simulated larger drawer weights, despite training being conducted only on an empty drawer. As shown in Fig. 4(D) and Movie S5, the time-aware policy again outperformed the baseline by executing careful and progressive pulls and recovering rapidly from transient slips. The ability to adjust motion tempo through time ratio thus serves as an implicit regulator that maintains stability

---

**Figure 4** (*preceding page*): **Time awareness improves stability and robustness to unseen dynamics.** (A) With more time available, the time-aware policy adopts cautious behaviors that (i) mitigate sim-to-real gaps (e.g., cube dynamics differences), (ii) generalize to unseen scenarios such as more granular media (40 × more) than in the training, (iii) avoid aggressive motions hitting controller limits, and (iv) reduce manipulation noise across all activities. (B)-(D) Zero-shot generalization tests in simulation. For granular media pouring, both vanilla and time-aware policies trained on one bean were zero-shot evaluated on 40 beans. The baseline policy poured aggressively, causing substantial spillage, while the time-aware policy adjusted its behavior according to the scheduled time, pouring carefully to ensure success. For drawer opening, both policies trained on empty drawers were evaluated under two physical property changes. With increased friction, the baseline policy repeatedly slipped and failed to recover, while the time-aware policy adapted by grasping firmly and pulling slowly. With added weight, the time-aware policy again demonstrated careful manipulation with fewer slips and strong recovery ability. (E) The time-aware policy consistently outperforms the baseline across all time ratios. No single time ratio achieves high success across tasks, indicating that neither purely aggressive nor purely conservative behavior handles task variations effectively. Adjustable time ratios enable the time-aware policy to maintain success under dynamic variations.

across a wide range of dynamic perturbations.

### **Interpreting the role of temporal observations**

To understand how time-aware signals shape decision-making, we visualized the policy’s internal responses to variations in remaining time and time ratio. We hypothesize that different temporal inputs alter which observations the policy prioritizes when generating actions. As shown in Fig. 5, we analyzed two key frames from the cube-stacking task, involving grasping and stacking, using action visualization and saliency analysis.

During the grasping phase (Fig. 5(A)), small time ratios produced counter-directed actions that decelerated movement for stable grasping, whereas large time ratios generated forward-directed, sliding motions toward the target cube. Similarly, shorter remaining time induced more aggressive actions denoted by arrows with larger magnitude, while greater remaining time led to gentle and deliberate trajectories. When time was limited, the time-aware policy focused narrowly on “local” variables, such as `cubeA_pos X`, `Y` and end-effector position. With more available time, the time-aware policy expanded its attention to additionally include `cubeA_pos Z`, translations between the cubes, time ratio, and remaining time, thereby enabling more planned and stable behaviors.

During stacking (Fig. 5(B)), increasing the remaining time (or equivalently lowering the time ratio) decelerated motion, ensuring precise alignment before release. Conversely, decreasing remaining time triggered fast, throw-like behaviors. Under tight schedules, the policy concentrated only on task-essential features to complete the action as quickly as possible, while with longer schedules it incorporated a broader set of spatial and temporal relations to achieve smooth and stable stacking, such as `cubeA pose`, inter-cube translations, end-effector pose, and remaining time.

Our analyses indicate that temporal signals dynamically reshaped the policy’s perceptual and control priorities. Time-aware conditioning acts not as a simple timing constraint, but as an internal mechanism that modulates observation importance to shape adaptive behaviors.

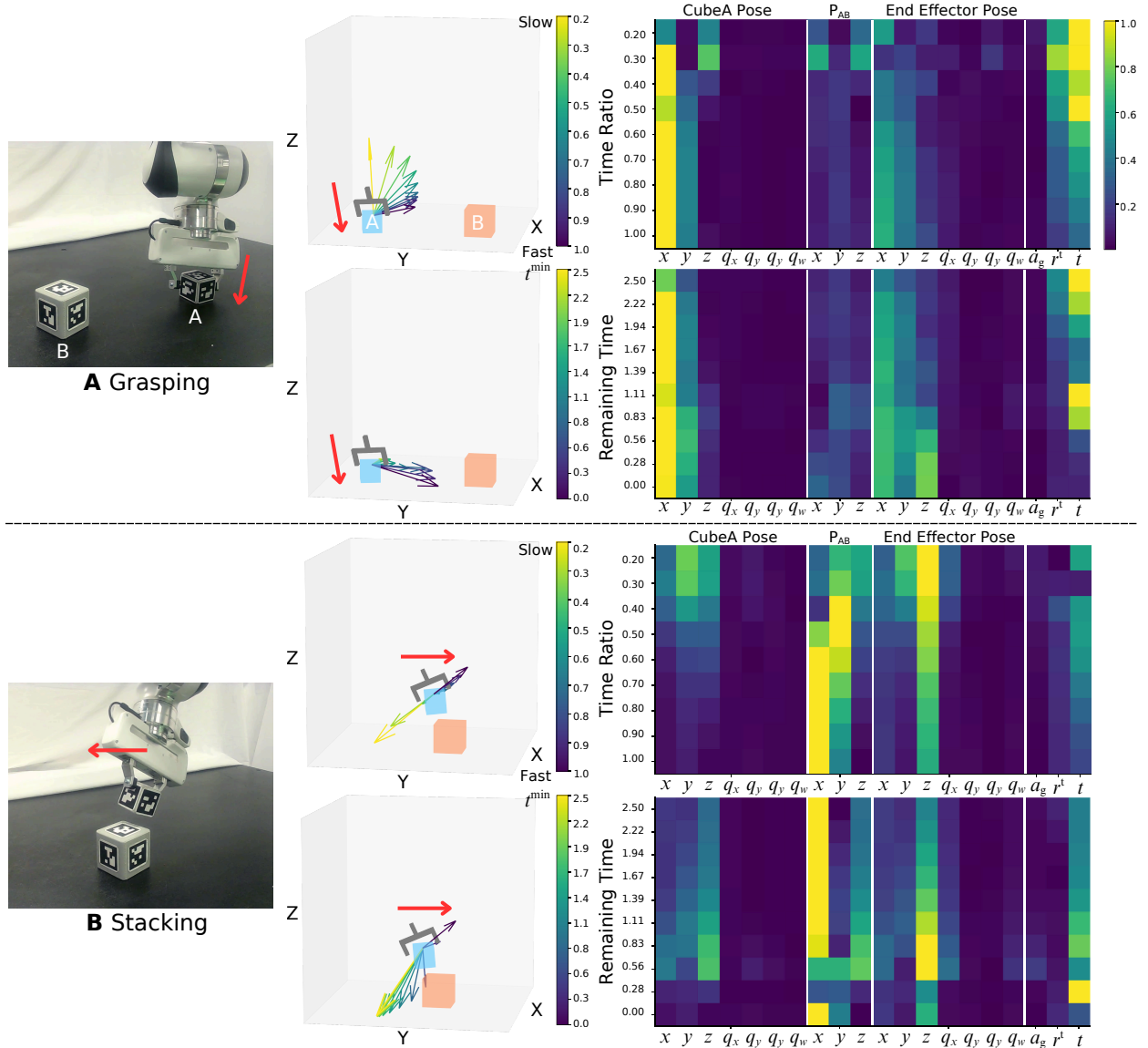


**Figure 5: Temporal observations modulate action generation and observation saliency.** We analyze the effect of temporal variables during two manipulation stages: (A) grasping and (B) stacking. Left: current real-world snapshots. Middle: actions under modified temporal observations (other observations held constant) at the current state, visualized in simplified 3D space. Right: heatmaps depicting changes in observation importance under the same temporal observation variations (i.e.,  $\frac{\partial \pi(a|s,T,tr)}{\partial s}$ ). Within each stage, the upper row shows effects of different time ratio values; the lower row shows effects of different remaining time. The time-aware policy adapts action selection based on both time ratio and remaining time. Variations in these temporal observations modulate attention allocated to different states during action generation.

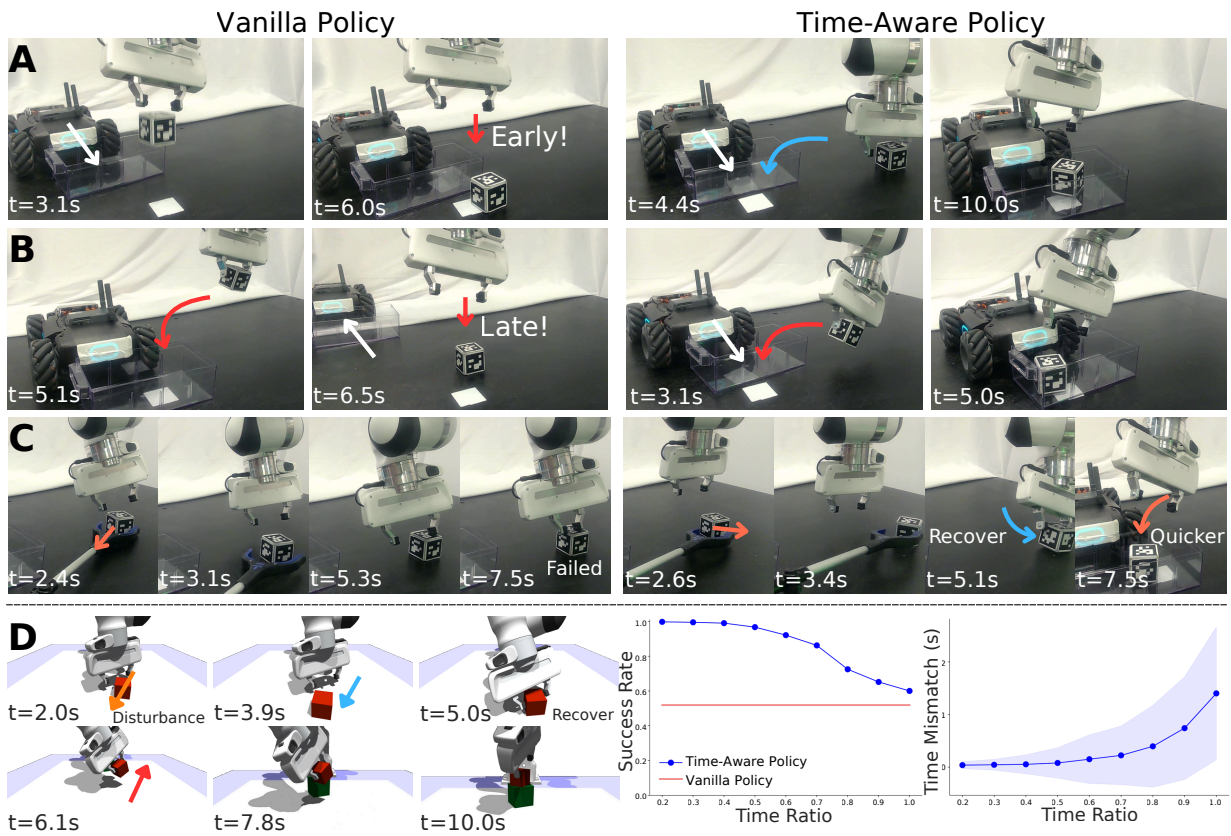


**Figure 6: Time-aware policy enables punctual and robust multi-agent collaboration.** (A) With a 10s schedule, the vanilla policy consistently released the object too early, whereas the time-aware policy delivered stably and punctually. (B) With a 5s schedule, the vanilla policy consistently missed the scheduled time, while the time-aware policy remained punctual. (C) Under disturbances, the time-aware policy exhibited robust recovery, whereas the baseline policy became stuck, significantly delaying collaboration and causing task failure. (D) Similar disturbances applied during cube stacking showed the time-aware policy quickly recovered and completed the task. Success rates remained consistently higher than baseline, particularly with more available time (i.e., smaller time ratios). Small time mismatches ( $< 1.5s$ ) under disturbance demonstrate that the time-aware policy compensates for recovery time through more efficient behaviors after recovery, which is a critical capability for real-world collaborative tasks.

## Collaboration and resiliency in multi-agent settings

To examine how time awareness supports coordination and reliability in multi-agent systems, we used object delivery task in which a robotic arm and a mobile vehicle must cooperatively deliver an object within a shared temporal schedule. This task exposes three central challenges.

First, the completion time of each agent is inherently uncertain. For example, the vehicle cannot anticipate how long the arm will take to transfer the object. Consequently, it must arrive early and wait, which can waste time and energy. Second, most existing methods lack a mechanism for online motion adaptation when timing requirements change. In our task, when the vehicle slows down or accelerates, the manipulator should correspondingly adjust its motion to synchronize the handover. Third, high reliability is essential for coordination under unexpected perturbations. Any failed recovery by one agent will cause a cascade delay for others. Traditional solutions depend on precise calibration and pre-defined synchronization logic, which are fragile to even minor deviations.

As illustrated in Fig. 6 (A, B, and C), the vanilla policy was extremely sensitive to small variations. When the vehicle’s scheduled arrival time was modified, the manipulator often released the box too early or too late, causing handover failure. When random disturbances occurred, such as external pushes, the arm failed to recover, and the entire collaborative sequence collapsed. These failures stemmed from the policy’s bias toward disturbance-free trajectories learned during training without explicit time awareness, leaving no capacity for adaptive re-scheduling.

The time-aware policy resolved these issues by explicitly reasoning about remaining time at every control steps. This naturally enabled two cooperative capabilities. First, the time-aware policy continuously reported its remaining-time estimate to the vehicle to allow the vehicle to plan its approaching speed. Second, it adapted to updated schedules in real time, even when the vehicle’s arrival time changed mid-execution.

We varied the vehicle’s travel duration between 5 s and 10 s per episode and found that the time-aware policy remained strictly punctual with an average delivery deviation of only 0.43 s (Fig. 6 (A, B, and C), Table 3). In contrast, the vanilla policy succeeded in only 2/10 trails and showed deviations exceeding several seconds. The time-aware policy’s punctuality ensured accurate and predictable object handover without any additional synchronization logic.

We next tested whether time awareness also enhances recovery under unforeseen perturbations.

Fixing the delivery deadline to 7.5 s, we randomly applied external pushes to the box object as the gripper approached (Fig. 6(D)). Despite the disturbance, the time-aware policy first executed a smooth re-grasp and subsequently accelerated to compensate for lost time, maintaining the same final schedule. Quantitatively, the time-aware policy achieved 7/10 successful recoveries with an average deviation of 0.45 s, while the vanilla policy failed in all disturbed trials (Table 3).

To analyze the mechanism in a controlled setting, we reproduced a similar disturbance in the cube-stacking task in simulation. When the gripper was within 5 cm of the source cube, we applied a 10 N planar force at the cube’s center for one simulation step to mimic unexpected contacts. After the disturbance, the agent was required to complete the task within the original schedule.

The vanilla policy was highly brittle. Its success rate dropped by 47.1% and it often became trapped during re-grasp attempts, unable to realign the object once out of its training distribution. In contrast, the time-aware policy remained robust, particularly under smaller time-ratio values ( $tr_t < 0.5$ ). Fig. 6(E) visualizes a representative trajectory. After missing the first grasp, the policy paused momentarily, executed a gentle re-approach, and then accelerated to finish punctually. When  $tr_t < 0.5$ , the final time mismatch remained below 0.32 s.

These results reveal two emergent strategies induced by time awareness: (i) cautious recovery, where the time-aware policy slows down to re-establish contact stability under time surplus, and (ii) temporal compensation, where it accelerates afterward to meet the original schedule. These behaviors demonstrate that explicit time awareness provides a unified mechanism for both coordination and resilience, allowing multi-agent systems to remain synchronized and successful under dynamic, uncertain, and perturbed conditions.

### **Human-in-the-loop temporal control for real-time behavior adaptation**

Most existing robot policies lack the ability to switch behaviors dynamically based on temporal context during execution, thereby neglecting how a task can be completed to suit different user preferences or environmental conditions. In industrial settings, users may prioritize minimal scheduled time to maximize throughput, whereas in household or human-collaborative environments, quieter and safer operation is often preferable. In contrast, the time-aware policy provides a unified mechanism for controlling task execution tempo through explicit temporal conditioning. By adjusting the time ratio, the same policy can smoothly transition between fast, dynamic, and cautious, stable

**Table 3: Evaluation of the Box Delivery Task.** This table presents the performance comparison between the vanilla policy and the time-aware policy for box delivery tasks under different task conditions. Success trials indicate the number of successful attempts out of 10, and time difference measures the deviation from the target time across all successful trials. The time-aware policy demonstrates strong punctuality and robustness to disturbances.

Box Delivery	Vanilla Policy		Time-aware Policy	
	Success Trials $\uparrow$	Time Diff (s) $\downarrow$	Success Trials $\uparrow$	Time Diff (s) $\downarrow$
Varied Time (5-10s)	2/10	-	<b>10/10</b>	<b>0.43 <math>\pm</math> 0.47</b>
Random Disturbance	0/10	-	<b>7/10</b>	<b>0.45 <math>\pm</math> 0.89</b>

behaviors. To demonstrate this flexibility, we implemented two complementary control strategies that exploit the continuous nature of time awareness:

- **Heuristic stage-wise control:** The manipulation process is divided into distinct stages. Each stage is assigned a tailored time ratio. Under the same total time constraint, the policy can act carefully in stages where caution and precision are critical (e.g., grasping, pouring, pulling or stacking) and aggressively where stability is less crucial (e.g., approaching or transporting).
- **Online interface control:** The user provides real-time time ratio via a simple and intuitive interface (e.g., keyboard or slider) to directly steer the behavior of the robot to align with high-level human intents.

In heuristic stage-wise control, we divided each manipulation task into several high-level stages based on task semantics (e.g., approach, grasp, transport, and stack). Each stage was assigned a binary execution mode (i.e., efficient (E) or stable (S)) and a proportion of the total scheduled time. Once the current stage exhausted its allocated temporal budget, the system automatically transitioned to the next stage and applied its associated time ratio.

To maintain a consistent total schedule while allowing each stage to operate at a different time ratio, we computed the relative scaling between the stable and efficient modes based on their assigned time portions. Intuitively, this heuristic ensures that stages labeled as stable (S) receive smaller time ratios to encourage slower and more cautious motions, while efficient stages (E) receive

larger ratios to encourage faster and dynamic motions, yet the overall duration remains unchanged. The exact formulation of this allocation rule, including how the ratio between stable and efficient phases is computed and bounded within valid limits, is provided in the Method: Heuristic stage-wise control details. A summary of the resulted parameters are shown in Table S1.

We conducted real-world stage-wise control for all three tasks. Qualitative results can be found in Movie S7. Fig. 7(C) illustrates a representative cube-stacking episode using the heuristic stage-wise control. A larger time ratio during approaching and transporting gave faster and more assertive motion, while a smaller time ratio during grasping and stacking induced slower and precise movements. Across trials, the time-aware policy consistently finished within the target schedule while reaching lower instability with smaller time ratio.

Since real-world scene instability is very difficult to measure and extremely noisy, to quantitatively evaluate the performance of stage-wise control, we used simulation for quantitative evaluations over all three tasks. Fig. 7(A) reports total instability measured during the stable stages. Under the same scheduled time, the time-aware policy with stage-wise control achieved substantially lower instability than constant-ratio control, which wastes time where cautious behaviors were not necessary such as approaching or transporting. Notably, the adaptive stage-wise behavior from the time-aware policy emerged without any training-time ratio randomization, demonstrating that explicit temporal conditioning alone suffices for fine-grained adaptation across long-horizon manipulation stages.

To further understand when stage-wise control is most beneficial, we analyzed the relationship between initial configuration and episode-level instability under both control modes. As shown in Fig. 7(B), the advantage of stage-wise control increased with manipulation distance. Longer-distance tasks required proportionally larger scheduled time, providing more absolute time for stability-critical phases and producing greater instability reduction per step.

As mentioned above, another way to enable human-in-the-loop control is to allow users to directly adjust time ratio in real time. In qualitative demonstrations shown in Fig. 7 (D and E), user interaction effectively corrected the robot’s behavior under unmodeled conditions. In granular pouring, an initially cautious policy caused beans to adhere to the cup. By increasing the time ratio, the user steered the robot’s motions to generate more vigorous pouring and ensured successful completion. In drawer opening, an initially aggressive pull saturated joint velocity limits and

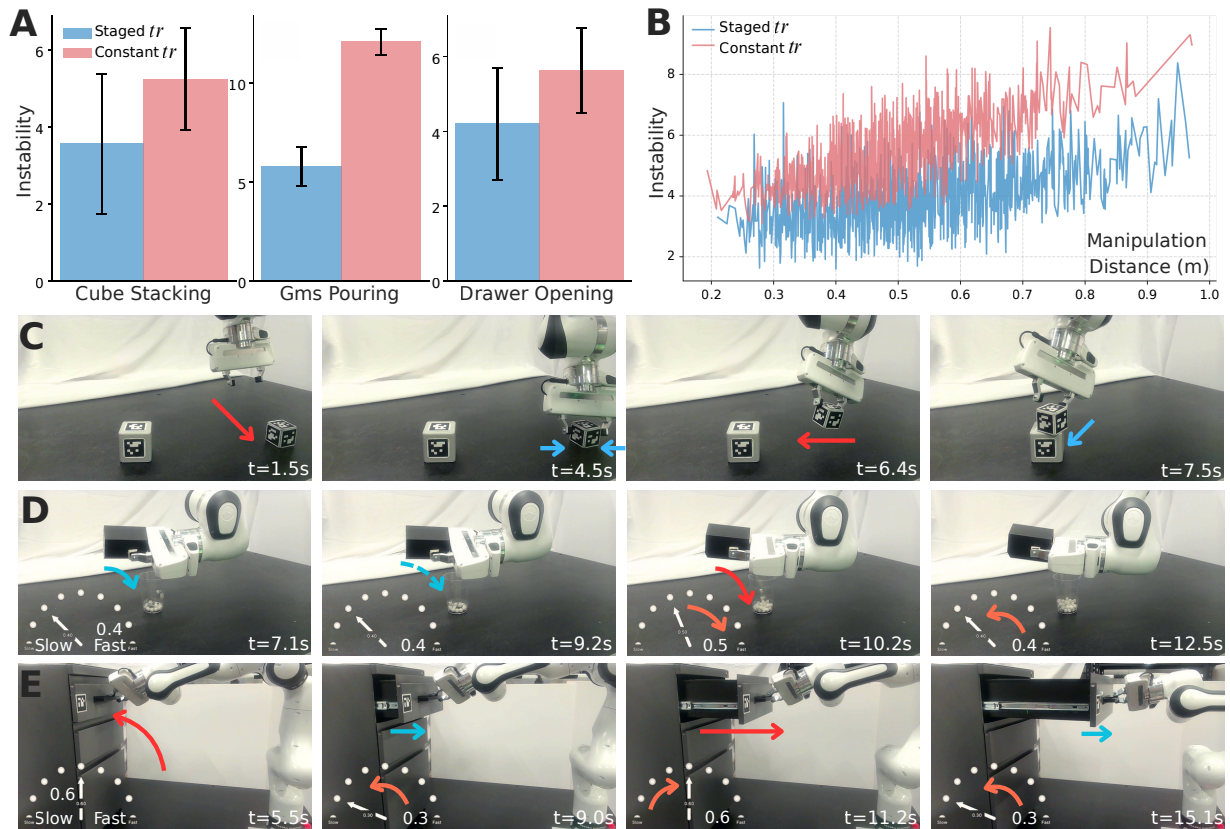


**Figure 7: Explicit time awareness enables stage-wise control and interactive online adjustment.**

(A) Stage-wise control allocated more time to contact-rich stages (e.g., grasping, stacking) and less time to other stages, enabling more careful behaviors and yielding markedly lower instability across tasks. (B) The benefit of stage-wise control increases with task horizon. For cube stacking, we defined manipulation distance as the initial gripper-to-cube distance plus cube-to-target distance. As this distance increased, stage-wise control achieved larger instability reductions under identical scheduled time. (C) Example episode for cube stacking. Large time ratios during approach and transport produced faster motions with higher instability tolerance; small time ratios during grasping and stacking yielded cautious, stable behavior. Tasks completed within the scheduled time while achieving higher stability and lower contact noise. (D)-(E) Real-time behavior adaptation via online interface control. In granular pouring, increasing the time ratio overcame media sticking from overly gentle actions. In drawer opening, reducing the time ratio during initial pulling, then gradually increasing it, mitigated initial lag and stabilized the low-level controller. This interface enables robot adaptation to new scenarios through high-level human feedback.

destabilized control. By decreasing the ratio early and increasing it later, the user enabled smooth initiation to start pulling, followed by efficient completion through acceleration later.

These results highlight the practical versatility of time awareness. A single policy, without re-training, accommodates both pre-programmed stage priorities and real-time human feedback, which can seamlessly balance efficiency, robustness, and safety. This capability offers a practical interface for deploying learned policies in diverse real-world settings where environmental variability and user intent demand adaptive and human-aligned robot behavior.

### **Ablation studies and additional baselines**

To verify that each component of our framework is essential for achieving the observed behaviors, we conducted a series of ablation and baseline experiments in simulation across all three tasks. Each variant used the same policy architecture, observation space, and scheduled time (i.e.,  $2t^{\min}$ ) as the full time-aware policy.

**Direct interpolation baseline.** To test whether simple temporal scaling of motion could achieve the same adaptability as our time-aware policy, we implemented an interpolation baseline. In this setting, we first trained a vanilla reinforcement learning policy without any of our time-aware components. We then slowed down its actions through joint-space interpolation. At each control step, the policy output was converted into a target joint configuration, which was then linearly interpolated into three intermediate configurations executed sequentially at the same control frequency (20 Hz) as the time-aware policy. All task parameters, environmental randomization, and success criteria followed those described in Section: Adaptive stability and environmental robustness. Each condition was evaluated over 2000 randomized simulation trials.

As shown in Fig. S1(A), although interpolation effectively slowed the robot’s motion, the resulting behaviors were nearly identical to those of the vanilla policy. The robot failed to adapt to varying contact dynamics or environmental disturbances. Cubes were often displaced during stacking, granular media spilled during pouring, and gripper slipped while pulling drawers. In contrast, the time-aware policy learned to modulate its motion dynamically through the control of time ratio. These adaptive behaviors enabled consistent and robust performance across environmental variations, achieving substantially higher success rates than the interpolated baselines. More real-world examples are shown in Movie S2.

**Without time and instability objectives.** We next removed both the time and instability objectives from training. To evaluate behavioral differences, we defined “active time” as the duration during which the manipulated object (i.e., cube, cup, or drawer) was moving. As shown in Fig. S1(B), the policy without these objectives exhibited short active time and high scene instability. The policy frequently idled and ignored temporal constraints. Adding only the time objective increased active manipulation and partially reduced instability by encouraging faster execution. Incorporating both objectives produced the intended balance: the policy utilized 62.2% more active time for purposeful interaction, reduced maximum instability, and still met the scheduled completion time. These results suggest that both objectives are jointly required for learning temporally efficient yet stable manipulation.

**Without constrained optimization.** Finally, we evaluated the effect of removing our constrained MDP (Method: Constrained Markov Decision Process) formulation by directly applying a dense penalty on instability. Since the resulting objective combined sparse task rewards, time rewards, and an instability term, we had to manually tune penalty scalings in this study. We searched five different scaling combinations, and each combination was trained with 3 different seeds. As illustrated in Fig. S1(C), training became highly sensitive to penalty scaling. Large penalty scaling reduced object interaction and could even break policy training, while small scaling failed to enforce the instability constraint effectively. Moreover, this tuning was required for each task. A scaling factor that was effective for one task (e.g., cube stacking) destabilized others (e.g., granular pouring). In contrast, our CMDP formulation automatically maintained stability without per-task tuning by treating instability as a constraint during policy optimization.

## Discussion

We introduced time-aware policy learning, a reinforcement learning framework that enable robot policies to explicitly perceive and reason about time. By embedding temporal awareness into both the learning objective and the policy representation, our approach allows robots to balance speed, stability, and adaptability in real time. The framework optimizes two complementary objectives: a minimum-time objective that encourages rapid task completion, enabling the policy to learn complex and dynamic manipulation skills, and a time-aware objective that promotes punctual and

context-reactive execution to steer its behavior. The product is a single policy capable of smooth behavior modulation across varying temporal constraints. Through simulation and real-world experiments, we showed that explicit time awareness unlocks a broad set of capabilities, ranging from robustness to disturbances, to generalization to unseen environments, and controllability through human input. Importantly, all of these emergent behaviors can be obtained through explicit time awareness without any re-training or reward adjustment during test time.

Our study highlights several conceptual lessons about how explicit time awareness embedded in policy learning can reshape robot control and learning. Time can act as a unifying variable to link with behavior, performance, stability, and resiliency. Rather than being treated as a fixed scheduling constraint, time becomes a controllable dimension of policy behavior. By conditioning on both the remaining time and the time ratio, our robot learns to accelerate and slow down accordingly, in order to achieve a trade-off between productivity and precision that emerges automatically from training.

Time awareness can enhance robustness and sim-to-real transfer. When real-world conditions differ from simulation, such as altered dynamics, increased friction, or added payload, the time-aware policy can adapt by modulating its internal tempo instead of re-learning from scratch. This temporal adaptation acts as a meta-stabilizing mechanism that allows the same policy to function reliably across domains.

Moreover, time awareness naturally supports multi-agent and human-in-the-loop control. By exposing the temporal progress of motions as an interpretable signal, the policy enables other robots or humans to anticipate task completion and synchronize behaviors. This transparency is critical in collaborative and shared-workspace environments, where mismatched timing often leads to inefficiency or safety risks.

Furthermore, time becomes an intuitive channel for human control. Our proposed time ratio interface allows users to adjust robot behavior in real time without modifying any low-level control inputs or even understanding the low-level control mechanisms. Increasing the ratio prompts faster and more assertive actions, and decreasing it induces caution and precision. This mechanism provides a minimal yet powerful means of embedding human preferences or contextual constraints into robot actions.

Our analyses reveal that time-awareness is not merely a scheduling constraint but a fundamental

factor that shapes how the policy perceives and processes environmental information. Time-aware policy learns to dynamically re-weight sensory and kinematic observations depending on both the remaining time and the current time ratio command. As shown in our ablation studies, our formulation of the constrained optimization process for the stability and time objective is critical for the successful training of our adaptive policy. Removing these components makes the policy ignore subtle cues about task progress and environmental dynamics. In contrast, the full formulation learns to prioritize spatial precision when time is abundant and task progress when time is scarce. These findings suggest that time awareness can restructure the internal representations of state and decision-making, linking time, perception, and control into a single coherent framework.

While our results demonstrate strong adaptability, robustness, and resiliency of time-aware policy learning, several limitations suggest directions for future progress. First, our stability measure using the sum of object linear velocities offers a coarse proxy for dynamics stability. Future work could integrate richer metrics such as acceleration, jerk, or force-based feedback, or learn data-driven stability estimators from multi-modal sensory streams. Second, each task in our work was trained with a separate time-aware policy. Extending the framework toward multi-task learning could yield shared temporal priors to accelerate adaptation to potentially novel tasks. We hypothesize that time-aware representations may offer an intuitive transfer avenue, providing a foundation for cross-task skill transfer.

Third, our policies rely on state-based observations since sensory observation is not our main focus. It's natural to integrate raw visual inputs or multimodal perception in future work to make the framework more robust to occlusion and improve real-world deployability. Finally, although our approach allows human users to adjust high-level timing, the mapping between time ratio changes and subjective task quality could be further explored. Studying how human operators interpret and use temporal control with large-scale human studies may contribute to the research avenue in time-based human-robot interaction.

Time-aware policy learning offers a new lens on robotic autonomy. It treats time not as a constraint but as a control dimension that mediates between efficiency, robustness, resiliency, and coordination. This perspective connects robotics with broader scientific questions about how intelligent agents perceive and allocate temporal resources. Beyond manipulation, similar principles could enhance locomotion, aerial coordination, assistive care, and tele-presence where timing and

synchronization are critical.

In the long term, we envision that time-awareness could serve as a foundational layer in the next-generation of robot learning systems that integrate planning, perception, reasoning, and human intent through temporal reasoning. By learning how fast and when to act, rather than merely what to do, robots can move closer to human-like fluency by executing actions that are not only successful but also punctual, adaptable, and intuitively aligned with their collaborators.

Overall, our results suggest that time-awareness may represent a fundamental axis of robot intelligence, enabling systems that self-regulate their speed, precision, and interaction in a continuously changing world.

## Materials and Methods

### Time-aware policy learning mathematical formulation

We formulate the time-aware policy under a constrained Markov decision process (CMDP) that jointly optimizes for task success, punctuality, and physical stability. The primary objective maximizes sparse task rewards and the punctuality objective for successful task completion within the scheduled time, while an auxiliary constraint enforces scene stability to ensure effective use of available time. An overview of the framework is illustrated in Fig. 2. The primary objectives have been discussed earlier in the manuscript. We therefore provide additional information on other formulations and constraints in this section.

**Define the instability objective.** Scene instability quantifies how dynamically unstable the environment is at each step. It is defined as the sum of velocities of all movable objects, excluding the robot itself:

$$p_t = \sum_{i=0}^J \|v_t^i\|_2, \tag{5}$$

where  $v_t^i \in \mathbb{R}^3$  is the translational velocity vector of the  $i$ -th movable object.

Directly penalizing instability overly constrained motion and suppressed interaction. To avoid this, we enforced stability as a constraint below a time-scaled threshold  $p^{\max} \cdot tr_t$ , where  $p^{\max}$  denotes the maximum allowed stability and is estimated alongside the temporal lower bound  $t^{\min}$  as described earlier. The resulting instability constraint at time step  $t$  is:

$$c_t^{\text{inst}} = \max(p_t - p^{\text{max}} \cdot tr_t, 0), \quad (6)$$

where  $p_t$  is the instability at  $t$  step. This constraint encourages the agent to act cautiously when ample time remains and allows the agent to act dynamically when time is limited.

**Embed temporal observations.** Before time-aware policy training, we incorporate two temporal signals (i.e., the remaining time  $T^{\text{left}}$  and the time ratio  $tr$ ) into the time-optimal policy without hurting its performance. To achieve this, we leverage behavior cloning with the following learning objective:

$$J_S(\pi) = \mathbb{E}_{a \sim \pi^*(\cdot | s)} \left[ \log \pi^*(a | s) - \log \pi(a | s, T^{\text{left}}, tr) \right], \quad (7)$$

where  $\pi^*$  is the time-optimal policy. At the beginning of each episode,  $tr$  was uniformly sampled from  $[0.2, 1]$  and kept fixed, while  $T^{\text{left}}$  evolves via Eq. 4. Training continues until the augmented policy converges and its performance does not exhibit more than 5% degradation.

**Constrained Markov decision process.** The objective of a standard Markov Decision Process (MDP) is to find an optimal policy  $\pi^*$  that maximizes the expected sum of discounted future rewards as defined in Eq. 1. However, such formulations do not account for safety or resource limitations. To incorporate these constraints, we followed the constrained MDP (CMDP) framework. A collection of cost signals can be provided as  $C = \{c_1, c_2, \dots, c_n\}$  where each cost can represent a specific constraint along with corresponding thresholds  $E = \{\epsilon_1, \epsilon_2, \dots, \epsilon_n\}$ . Each cost function assigns a penalty to the transition  $(s, a, s')$  as  $c_i : S \times A \times S \rightarrow \mathbb{R}$ . An admissible policy must maximize the expected discounted return while ensuring that the discounted cumulative cost of every cost signal  $c_i$  does not exceed its threshold  $\epsilon_i$ . Formally, the agent solves:

$$\begin{aligned} \max_{\pi} \quad & J_R(\pi) \\ \text{s.t.} \quad & J_{C_i}(\pi) \leq \epsilon_i, \forall i \in \{1, \dots, n\}, \end{aligned} \quad (8)$$

where

$$J_{C_i}(\pi) = \mathbb{E} \left[ \sum_{t=0}^{\infty} \gamma^t c_i(s_t, a_t, s_{t+1}) \right]. \quad (9)$$

Following prior works (41, 42), this constrained policy optimization problem can be reformu-

lated as:

$$\begin{aligned} \max_{\pi'} \quad & \mathbb{E} [A_{R,t}^\pi(s, a)] \\ \text{s.t.} \quad & \underbrace{J_{C_i}(\pi) + \frac{1}{1-\gamma} \mathbb{E}_{\pi'} [A_{C_i,t}^\pi(s, a)]}_{J_{C_i}(\pi')} \leq \epsilon_i, \quad \forall i, \end{aligned} \quad (10)$$

where  $\pi$  denotes the current policy,  $\pi'$  denotes the updated policy, and  $A_{R,t}^\pi(s, a)$  and  $A_{C_i,t}^\pi(s, a)$  are unbiased estimators of the reward advantage and the  $i$ -th cost advantage at time step  $t$ , respectively,

In our formulation, the task success and punctuality objectives (Eq. 4) are represented as sparse rewards, while the instability (Eq. 6) is formulated as a constraint. This design offers several advantages. First, it eliminates the need to manually tune reward–cost trade-offs between objectives, thereby preventing unstable learning dynamics or collapse caused by improper scaling. Second, it allows us to employ separate critics for reward and cost estimation. This separation improves prediction accuracy, prevents interference between objectives, and enables independent normalization. Therefore, these benefits can stabilize gradient updates and mitigate the effect of magnitude differences across objectives. Finally, our formulation allows distinct discounting strategies for different objectives. To avoid premature convergence or reward vanishing, sparse rewards use no discount. Dense costs from instability can adopt a relatively small discount factor to reduce variance.

The overall objective is defined in Eq. 8 and further specified as

$$\begin{aligned} J_R(\pi) &= \mathbb{E} [\mathbb{1}_{\text{success}} \cdot \max(R - c^{\text{time}}, 0)], \\ J_C(\pi) &= \mathbb{E} \left[ \sum_{t=0}^N \gamma_c^t c_t^{\text{inst}} \right], \end{aligned} \quad (11)$$

where  $R$  denotes the sparse task success reward,  $c^{\text{time}}$  is the cost of the punctuality objective (Eq. 4),  $c_t^{\text{inst}}$  is the cost of instability constraint (Eq. 6), and  $\gamma_c$  is the discount factor of the cost. By clamping the sparse reward terms to remain nonnegative, we ensured that task success incentives are not eliminated by the cost. Overall, the objective function ensures task success, punctual completion, and the effective use of the available time.

**Loss function.** We optimize the time-aware policy with Penalized Proximal Policy Optimization (P3O) (42). P3O extends the standard Proximal Policy Optimization (PPO) algorithm (43) by adding explicit penalty terms for constraint violations, ensuring that cost thresholds are respected

during training. This approach balances reward maximization and constraint satisfaction within a unified proximal framework, and avoids instability caused by alternating or Lagrangian updates.

The overall P3O loss is:

$$L^{P3O}(\theta') = L_R^{\text{CLIP}}(\theta') - \sum_i \kappa_i \cdot \max \left\{ 0, L_{C_i}^{\text{VIOL}}(\theta') \right\}, \quad (12)$$

where  $\kappa_i$  controls the penalty strength for each constraint. The first term encourages reward improvement, while the second term suppresses any policy updates that increase cumulative cost beyond the threshold. Specifically, the first term  $L_R^{\text{CLIP}}(\theta')$  is the objective function of the original PPO algorithm:

$$L_R^{\text{CLIP}}(\theta') = \mathbb{E}_t \left[ \min \left( r_t(\theta') A_{R,t}^{\pi_{\theta'}}, \mathbf{Clip}(r_t(\theta')) A_{R,t}^{\pi_{\theta}} \right) \right], \quad (13)$$

where  $r_t(\theta')$  denotes the action probability ratio of the new policy and the current policy  $\frac{\pi_{\theta'}(a_t|s_t)}{\pi_{\theta}(a_t|s_t)}$ ,  $A_{R,t}^{\pi_{\theta}}$  denotes the reward advantage,  $\mathbf{Clip}(\cdot)$  denotes the ratio clip between  $[1 - \delta, 1 + \delta]$ , and  $\delta$  controls the policy update steps.

The second term defines the constraint objective:

$$L_{C_i}^{\text{VIOL}}(\theta') = L_{C_i}^{\text{CLIP}}(\theta') + (1 - \gamma_c)(J_{C_i}(\pi_{\theta'}) - \epsilon_i), \quad (14)$$

$$L_{C_i}^{\text{CLIP}}(\theta') = \mathbb{E}_t \left[ \max \left( r_t(\theta') A_{C_i,t}^{\pi_{\theta'}}, \mathbf{Clip}(r_t(\theta')) A_{C_i,t}^{\pi_{\theta}} \right) \right], \quad (15)$$

where  $\gamma_c$  is the discount factor of the cost, and  $A_{C_i,t}^{\pi_{\theta}}$  denotes the cost advantage.

Since the unnormalized  $A_{R,t}^{\pi_{\theta}}$  and  $A_{C_i,t}^{\pi_{\theta}}$  have different magnitudes, direct optimization may bias updates toward objectives with larger numerical scales. We therefore normalize both advantages to improve the policy learning. To ensure the constraint objective (i.e.,  $\mathbb{E}_t \left[ A_{C_i,t}^{\pi_{\theta}} \right] + (1 - \gamma_c)(J_{C_i}(\pi_{\theta}) - \epsilon_i) \leq 0$ ) remains unchanged, we adopt the same cost objective from prior work (44):

$$L_{C_i}^{\text{N-VIOL}}(\theta') = L_{C_i}^{\text{N-CLIP}}(\theta') + (1 - \gamma_c) \frac{(J_{C_i}(\pi_{\theta'}) - \epsilon_i) + \mu_{C_i}}{\sigma_{C_i}}, \quad (16)$$

$$L_{C_i}^{\text{N-CLIP}}(\theta') = \mathbb{E}_t \left[ \max \left( r_t(\theta') \tilde{A}_{C_i,t}^{\pi_{\theta'}}, \mathbf{Clip}(r_t(\theta')) \tilde{A}_{C_i,t}^{\pi_{\theta}} \right) \right], \quad (17)$$

$$\tilde{A}_{C_i,t}^{\pi_{\theta}} = \frac{A_{C_i,t}^{\pi_{\theta}} - \mu_{C_i}}{\sigma_{C_i}}, \quad (18)$$

where  $\mu_{C_i}$  and  $\sigma_{C_i}$  are the mean and standard deviations of  $A_{C_i,t}^{\pi_{\theta}}$ . This normalization keeps the optimization scale consistent and allows the policy to learn stably across multiple cost constraints.

Therefore, the normalized P3O objective then becomes:

$$L^{\text{N-P3O}}(\theta') = L_R^{\text{N-CLIP}}(\theta') - \sum_i \kappa_i \cdot \max \left\{ 0, L_{C_i}^{\text{N-VIOL}}(\theta') \right\}, \quad (19)$$

The final loss combines the normalized P3O objective with value and cost critic regressions and an entropy bonus to encourage policy exploration:

$$L(\theta') = c_1 L^{\text{C-V}}(\theta') + c_2 L^{\text{C-C}}(\theta') - c_3 L^{\text{H}}(\theta') - L^{\text{N-P3O}}(\theta') \quad (20)$$

with

$$L^{\text{C-V}}(\theta') = \mathbb{E}_t \left[ \left( V_{\theta'}^R(s_t) - G_t^R \right)^2 \right], \quad (21)$$

$$L^{\text{C-C}}(\theta') = \mathbb{E}_t \left[ \left( V_{\theta'}^C(s_t) - G_t^C \right)^2 \right], \quad (22)$$

$$L^{\text{H}}(\theta') = \mathbb{E}_t \left[ \mathcal{H}[\pi_{\theta'}](s_t) \right], \quad (23)$$

where  $V_{\theta'}^R(s_t)$  is the critic for the state value,  $V_{\theta'}^C(s_t)$  is the critic for the state cost,  $G_t^R$  is the cumulative return,  $G_t^C$  is the cumulative cost, and  $\mathcal{H}[\pi_{\theta'}](s_t)$  is the policy entropy at state  $s_t$ . The separate critics ensure accurate value and constraint estimation, and the entropy term maintains action diversity to prevent premature convergence.

## Implementation details

**Policy design.** The model architecture and control loop are illustrated in Fig. S2. The actor, value critic, and cost critic were implemented as 5-layer multilayer perceptrons (MLPs) with identical hidden dimensions but independent weights. The actor takes in task-related observations, robot states, observed remaining time  $t^{\text{left}}$ , time ratio  $r^t$ , and the previous commanded actions. The output defines the parameters  $\alpha \in \mathbb{R}^7$  and  $\beta \in \mathbb{R}^7$  of a Beta distribution,  $Beta(\alpha, \beta)$ . From this distribution, six continuous values are sampled to define end-effector motion in 6-DoF space, and one binary variable is sampled for gripper open/close control. The sampled actions are converted to target joint positions for the low-level joint impedance controller, and the sampled gripper action is applied to the gripper control.

Accurate scene instability and maximum allowable instability are difficult to measure for real-world deployments, yet are essential for estimating state values. To bridge this gap, we employ an

asymmetric actor–critic method. The critic observes both noise-free observations and additional privileged information, such as instability metrics and task-specific privileges (e.g., granular media positions in the pouring task), while the actor only uses noisy and observable inputs. The value critic output state value estimates, while the cost critic output state cost estimates. This design allows the actor to learn a deployable policy under partial observability, while the critic leverages privileged information to shape more accurate gradients. As a result, our learned time-aware policy can generalize to real robots in a zero-shot manner, requiring no additional fine-tuning or distillation.

**Training details.** Our training involves two stages corresponding to the learning of 1) the temporal lower bound policy and 2) the time-aware policy. In the first stage, we continue the training of a vanilla reinforcement learning policy using a modified reward function that emphasized time-optimal completion. To ensure accurate state-value estimation after reward modification, the critic network is reinitialized while reusing the pretrained actor, consistent with recent findings in reinforcement learning (45, 46, 47, 48, 49). During the first  $N$  iterations, only the critic is updated to stabilize value predictions before allowing joint updates with the actor. Because this setting uses sparse rewards, we employ a KL-divergence constraint to prevent policy collapse. After each gradient step, if the KL divergence between the old and new policy exceeds a threshold (e.g., 5), the update will be reverted. This safeguard maintains a bounded trust region for stable on-policy learning.

In the second stage of learning the time-aware policy, for each episode, we randomly sample environment configurations along with corresponding  $(t^{\min}, p^{\max})$  pairs obtained from the lower-bound estimation stage. The time ratio  $tr$  is uniformly sampled from  $[0.2, 1]$  and held constant within an episode, while the remaining time  $T^{\text{left}}$  is updated according to Eq. 4. We keep the KL-divergence mechanism to ensure stability during training.

**Sim-to-real transfer.** To ensure robust sim-to-real transfer, we conducted standard joint-level system identification before training the vanilla policy. Each joint’s position limits, maximum velocity, and maximum allowable torque were measured on the real robot and imposed as hard limits in simulation. We also characterized the gripper joint’s actuation delay and incorporated this latency into the simulator. During deployment, to mitigate drift caused by joint tracking latency on the real robot, commanded joint angles at each timestep were computed by incrementally adding the policy’s predicted offset to the previous commanded joint angles rather than the most recent

measured positions. The policy ran at 20 Hz for the arm and 2 Hz for the gripper in both simulation and real world, while the low-level impedance controller operated at 1 kHz. To address real-world state estimation and measurement noise, we injected noise into the actor’s observation for all policy trainings. Detailed noise settings are provided in the Supplementary Material Table S4.

### Heuristic stage-wise control details

Based on our earlier discussions on enabling human-in-the-loop control of the time-aware policy through heuristic stage-wise control, we discuss the details on how to calculate the stage-wise time ratios. Each stage is assigned a binary execution mode (i.e., efficient (E) or stable (S)) and allocated a proportion  $P_i$  of the total scheduled time  $t^{\text{goal}}$ . The system will automatically transition to the next stage once the allocated time for the current stage is exhausted, updating the active time ratio accordingly. To ensure the total scheduled duration remained constant and all time ratios stay within valid bounds, we first compute the ratio of allocated time proportions between stable and efficient stages:

$$k = \frac{\sum_{i=1}^M \mathbb{1}[\text{Stage}_i = \text{S}] \cdot P_i}{\sum_{i=1}^M \mathbb{1}[\text{Stage}_i = \text{E}] \cdot P_i} \quad (24)$$

where  $M$  is the total number of stages and  $P_i$  is the time portion of  $i$ -th stage. Based on this ratio, the time ratio for stable and efficient stages can be computed as:

$$\bar{r}^t = \frac{t^{\text{min}}}{t^{\text{goal}}}, \quad \Delta r_S^t = \min\left(\bar{r}^t - r_{\text{min}}^t, \frac{r_{\text{max}}^t - \bar{r}^t}{k}\right), \quad \Delta r_E^t = k \cdot \Delta r_S^t, \quad (25)$$

and

$$r_E^t = \bar{r}^t + \Delta r_E^t, \quad r_S^t = \bar{r}^t - \Delta r_S^t. \quad (26)$$

Here,  $t^{\text{min}}$  is the temporal lower bound,  $r_{\text{min}}^t$  and  $r_{\text{max}}^t$  denote the valid range of the time ratio, and  $(r_S^t, r_E^t)$  correspond to the time ratios for the stable and efficient stages, respectively. Our formulation guarantees that stable stages operate with a reduced time ratio (favoring caution and precision), while efficient stages use an elevated ratio (favoring speed), while maintaining the scheduled time. The complete stage definitions for all tasks are listed in Table S1.

## References and Notes

1. K. E. v. Baer, *Welche Auffassung der lebenden Natur ist die Richtige?* (1908).
2. E. Pöppel, Time perception, in *Perception* (Springer), pp. 713–729 (1978).
3. P. G. Zimbardo, J. N. Boyd, Putting time in perspective: A valid, reliable individual-differences metric, in *Time perspective theory; review, research and application: Essays in honor of Philip G. Zimbardo* (Springer), pp. 17–55 (2014).
4. M. Maniadakis, P. Trahanias, Time models and cognitive processes: a review. *Frontiers in neurorobotics* **8**, 7 (2014).
5. J. Hu, *et al.*, Flare: Achieving masterful and adaptive robot policies with large-scale reinforcement learning fine-tuning, in *2025 IEEE International Conference on Robotics and Automation (ICRA)* (IEEE) (2025), pp. 3617–3624.
6. M. Yang, *et al.*, Anyrotate: Gravity-invariant in-hand object rotation with sim-to-real touch. *arXiv preprint arXiv:2405.07391* (2024).
7. W. Huang, I. Mordatch, P. Abbeel, D. Pathak, Generalization in dexterous manipulation via geometry-aware multi-task learning. *arXiv preprint arXiv:2111.03062* (2021).
8. C. Liu, *et al.*, Robot Manipulation of Dynamic Object with Vision-Based Reinforcement Learning, in *2024 9th International Conference on Control and Robotics Engineering (ICCRE)* (IEEE) (2024), pp. 21–26.
9. B. Beigomi, Z. H. Zhu, Towards Real-World Efficiency: Domain Randomization in Reinforcement Learning for Pre-Capture of Free-Floating Moving Targets by Autonomous Robots, in *2024 IEEE International Conference on Robotics and Automation (ICRA)* (IEEE) (2024), pp. 11753–11759.
10. X. Liu, Y. Liu, Z. Liu, P. Huang, Unified human–robot–environment interaction control in contact-rich collaborative manipulation tasks via model-based reinforcement learning. *IEEE Transactions on Industrial Electronics* **70** (11), 11474–11482 (2022).

11. S. M. Rahman, Machine learning-based cognitive position and force controls for power-assisted human–robot collaborative manipulation. *Machines* **9** (2), 28 (2021).
12. S. Gu, *et al.*, A human-centered safe robot reinforcement learning framework with interactive behaviors. *Frontiers in Neurorobotics* **17**, 1280341 (2023).
13. J. Tobin, *et al.*, Domain randomization for transferring deep neural networks from simulation to the real world, in *2017 IEEE/RSJ international conference on intelligent robots and systems (IROS)* (IEEE) (2017), pp. 23–30.
14. J. Tremblay, *et al.*, Training deep networks with synthetic data: Bridging the reality gap by domain randomization, in *Proceedings of the IEEE conference on computer vision and pattern recognition workshops* (2018), pp. 969–977.
15. I. Akkaya, *et al.*, Solving rubik’s cube with a robot hand. *arXiv preprint arXiv:1910.07113* (2019).
16. X. B. Peng, M. Andrychowicz, W. Zaremba, P. Abbeel, Sim-to-real transfer of robotic control with dynamics randomization, in *2018 IEEE international conference on robotics and automation (ICRA)* (IEEE) (2018), pp. 3803–3810.
17. J. Tan, *et al.*, Sim-to-real: Learning agile locomotion for quadruped robots. *arXiv preprint arXiv:1804.10332* (2018).
18. A. Petrenko, A. Allshire, G. State, A. Handa, V. Makoviychuk, Dexpbt: Scaling up dexterous manipulation for hand-arm systems with population based training. *arXiv preprint arXiv:2305.12127* (2023).
19. J. Singla, A. Agarwal, D. Pathak, Sapg: split and aggregate policy gradients. *arXiv preprint arXiv:2407.20230* (2024).
20. Y. Narang, *et al.*, Factory: Fast contact for robotic assembly. *arXiv preprint arXiv:2205.03532* (2022).
21. B. Tang, *et al.*, Industreal: Transferring contact-rich assembly tasks from simulation to reality. *arXiv preprint arXiv:2305.17110* (2023).

22. R. Wilcox, S. Nikolaidis, J. Shah, Optimization of temporal dynamics for adaptive human-robot interaction in assembly manufacturing. *Robotics* **8**, 441 (2013).
23. F. Rea, A. Vignolo, A. Sciutti, N. Noceti, Human motion understanding for selecting action timing in collaborative human-robot interaction. *Frontiers in Robotics and AI* **6**, 58 (2019).
24. F. Cini, T. Banfi, G. Ciuti, L. Craighero, M. Controzzi, The relevance of signal timing in human-robot collaborative manipulation. *Science Robotics* **6** (58), eabg1308 (2021).
25. F. Pardo, A. Tavakoli, V. Levdik, P. Kormushev, Time limits in reinforcement learning, in *International Conference on Machine Learning* (PMLR) (2018), pp. 4045–4054.
26. Y. J. Kim, M. Chi, Time-aware deep reinforcement learning with multi-temporal abstraction. *Applied Intelligence* **53** (17), 20007–20033 (2023).
27. C. S. V. Gutiérrez, L. U. S. Juan, I. Z. Ugarte, V. M. Vilches, Time-sensitive networking for robotics. *arXiv preprint arXiv:1804.07643* (2018).
28. T. Kagawa, *et al.*, A study on latency-guaranteed multi-hop wireless communication system for control of robots and drones, in *2017 20th International Symposium on Wireless Personal Multimedia Communications (WPMC)* (IEEE) (2017), pp. 417–421.
29. F. Mastrogiovanni, A. Paikan, A. Sgorbissa, Semantic-aware real-time scheduling in robotics. *IEEE Transactions on Robotics* **29** (1), 118–135 (2012).
30. W. Grass, T. H. C. Nguyen, Improved response-time bounds in fixed priority scheduling with arbitrary deadlines. *Real-Time Systems* **54** (1), 1–30 (2018).
31. S. Baek, J. Baek, J. Choi, S. Han, A reinforcement learning-based adaptive time-delay control and its application to robot manipulators, in *2022 American Control Conference (ACC)* (IEEE) (2022), pp. 2722–2729.
32. M. Jin, J. Kim, J. Lee, P. H. Chang, Improving time-delay control for robot manipulators using TSK fuzzy logic control systems, in *2017 IEEE International Conference on Advanced Intelligent Mechatronics (AIM)* (IEEE) (2017), pp. 1743–1748.

33. A. Umbrico, A. Cesta, A. Orlandini, Human-aware goal-oriented autonomy through ROS-integrated timeline-based planning and execution, in *2023 32nd IEEE International Conference on Robot and Human Interactive Communication (RO-MAN)* (IEEE) (2023), pp. 1164–1169.
34. M. Maniadakis, E. Hourdakos, P. Trahanias, Time-informed task planning in multi-agent collaboration. *Cognitive Systems Research* **43**, 291–300 (2017).
35. M. Maniadakis, *et al.*, Time-aware multi-agent symbiosis. *Frontiers in Robotics and AI* **7**, 503452 (2020).
36. G. Li, J. Wu, Y. He, Act Better by Timing: A timing-Aware Reinforcement Learning for Autonomous Driving. *arXiv preprint arXiv:2406.13223* (2024).
37. Y. Jia, J. Xu, D. Jayaraman, S. Song, Dynamic grasping with a learned meta-controller, in *2024 IEEE 20th International Conference on Automation Science and Engineering (CASE)* (IEEE) (2024), pp. 3608–3615.
38. R. S. Sutton, A. G. Barto, *et al.*, *Reinforcement learning: An introduction*, vol. 1 (MIT press Cambridge) (1998).
39. V. Makoviychuk, *et al.*, Isaac gym: High performance gpu-based physics simulation for robot learning. *arXiv preprint arXiv:2108.10470* (2021).
40. Y. Zhu, *et al.*, robosuite: A modular simulation framework and benchmark for robot learning. *arXiv preprint arXiv:2009.12293* (2020).
41. E. Altman, *Constrained Markov decision processes* (Routledge) (2021).
42. L. Zhang, *et al.*, Penalized proximal policy optimization for safe reinforcement learning. *arXiv preprint arXiv:2205.11814* (2022).
43. J. Schulman, F. Wolski, P. Dhariwal, A. Radford, O. Klimov, Proximal policy optimization algorithms. *arXiv preprint arXiv:1707.06347* (2017).
44. J. Lee, *et al.*, Evaluation of constrained reinforcement learning algorithms for legged locomotion. *arXiv preprint arXiv:2309.15430* (2023).

45. W. Xiao, *et al.*, Efficient Online RL Fine Tuning with Offline Pre-trained Policy Only. *arXiv preprint arXiv:2505.16856* (2025).
46. M. Cho, J. Park, J. Kim, Y. Sung, ARS: Adaptive Reward Scaling for Multi-Task Reinforcement Learning, in *Forty-second International Conference on Machine Learning*.
47. H. Sun, *et al.*, Exploit reward shifting in value-based deep-rl: Optimistic curiosity-based exploration and conservative exploitation via linear reward shaping. *Advances in neural information processing systems* **35**, 37719–37734 (2022).
48. H. Ahn, J. Hyeon, Y. Oh, B. Hwang, T. Moon, Reset & distill: A recipe for overcoming negative transfer in continual reinforcement learning. *arXiv preprint arXiv:2403.05066* (2024).
49. M. Wołczyk, *et al.*, Fine-tuning reinforcement learning models is secretly a forgetting mitigation problem. *arXiv preprint arXiv:2402.02868* (2024).

## Acknowledgments

**Funding:** This work is supported by DARPA TIAMAT program under award HR00112490419, ARO under award W911NF2410405, and ARL STRONG program under awards W911NF2320182, W911NF2220113, and W911NF242021.

**Author contributions:** B.C., Y.J. conceived and designed the research. Y.J. performed simulations and physical experiments. All authors analyzed data and wrote the manuscript.

**Competing interests:** Duke University has filed patent rights for the technology associated with this manuscript. For further license rights, including using the patent rights for commercial purposes, please contact Duke’s Office for Translation and Commercialization (otcquestions@duke.edu) and reference OTC DU9041PROV.

**Data and materials availability:** The code is available at [https://drive.google.com/drive/folders/1sCfGEupQoO3WC7Iq4Qb0ysiXgS5o5L7w?usp=drive\\_link](https://drive.google.com/drive/folders/1sCfGEupQoO3WC7Iq4Qb0ysiXgS5o5L7w?usp=drive_link).

The high-resolution version of all the supplementary videos can be accessed at [https://drive.google.com/drive/folders/1UZq4122AkPZ0vdQmO9ffb7DzUEUgZ97c?usp=drive\\_link](https://drive.google.com/drive/folders/1UZq4122AkPZ0vdQmO9ffb7DzUEUgZ97c?usp=drive_link).

## Supplementary materials

Materials and Methods

Supplementary Text

Tables S1 to S4

Figs. S1 to S3

**Supplementary Movie S1 — Overview:** Overview of the motivation, key idea, and demonstrations.

**Supplementary Movie S2 — Baseline Interpolation:** Direct interpolation of vanilla RL policy without temporal awareness.

**Supplementary Movie S3 — Optimized Efficiency:** Time awareness enables faster task completion while maintaining punctuality at minimum scheduled time ( $tr_t = 1.0$ ).

**Supplementary Movie S4 — Flexible Punctuality:** Time awareness adapts behavior to meet variable deadlines across different scheduled times ( $0 < tr_t < 1$ ).

**Supplementary Movie S5 — Robust Adaptation:** Time awareness enhances stability and performance under varying environmental conditions.

**Supplementary Movie S6 — Coordinated Delivery:** Multiple agents collaboratively transport objects using time-aware coordination.

**Supplementary Movie S7 — Interactive Control:** Human-in-the-loop temporal control for real-time behavior adaptation.

# Supplementary Materials for Time-Aware Policy Learning for Adaptive and Punctual Robot Control

Yinsen Jia<sup>1</sup>, Boyuan Chen<sup>1,2,3\*</sup>

<sup>1</sup>Department of Electrical and Computer Engineering, Duke University

<sup>2</sup>Department of Mechanical Engineering and Materials Science, Duke University

<sup>3</sup>Department of Computer Science, Duke University

\*To whom correspondence should be addressed; Email: boyuan.chen@duke.edu.

## **This PDF file includes:**

Materials and Methods

Supplementary Text

Tables S1 to S4

Figures S1 to S3

## Materials and Methods

**Table S1: Stage-Wise Control Parameters for Different Tasks.** This table lists, for each task, the sequence of stages, the stage modes, the relative time portion per stage, and the total scheduled time. Efficient mode (E) encourages the policy to act faster, and stable mode (S) encourages the policy to act more cautiously. The time portion values represent the proportion of the total scheduled time allocated to each stage.

Task Name	Stage Name	Stage Mode	Time Portion	Scheduled Time
Cube Stacking	Approach, Grasp, Transport, Stack	E, S, E, S	0.15, 0.35, 0.15, 0.35	$2t^{\min}$
GM Pouring	Transport, Pour	E, S	0.5, 0.5	$2t^{\min}$
Drawer Opening	Approach, Grasp, Pull, Open	E, S, E, S	0.2, 0.2, 0.3, 0.3	$2t^{\min}$

**Table S2: Default Training Hyperparameters.** This table lists the hyperparameters used for training the policy with PPO algorithm, including their values and descriptions.

Hyperparameter	Value	Description
Learning Rate	0.0002	Learning rate
Num Envs	16384	The number of parallel simulation envs
$\Delta t$	1/60	The simulation step time
Roll-out Steps	32	The number of roll-out steps per update
Batch Size	131072	Batch size
Update Epochs	5	Update epochs
$\gamma$	0.995	The discount factor of the reward
$\lambda_{gae}$	0.95	The discount for GAE
$\epsilon$	0.2	The surrogate clipping coefficient
$c_1$	0.5	The coefficient of the value function
$c_3$	0.005	The coefficient of the entropy
$gclip_{max}$	0.5	Gradient clipping
Hidden Layer Size	[256, 128, 64]	The number of units
$R$	1000	Task Success reward

**Table S3: Time-Aware Training Stage Overrides.** This table lists the hyperparameter overrides specifically used for time-aware training stages, including their values and descriptions.

Hyperparameter	Value	Description
$\gamma$	1	The discount factor of the reward
$\gamma_c$	0.99	The discount factor of the cost
$c_2$	1.0	The coefficient of the cost function
$R_t$	100	The reward scale of the time objective

**Table S4: Details of Noise.** This table lists the noise levels applied to different observations across various task categories and robot states. The noise was uniformly sampled within the specified ranges.

Category Name	Observation Name	Unit	Level
Cube Stacking	CubeA Pos	m	$\mathcal{U}(\pm 0.01)$
	CubeA Rot	rad	$\mathcal{U}(\pm \pi/60)$
	CubeB Pos	m	$\mathcal{U}(\pm 0.01)$
	CubeB Rot	rad	$\mathcal{U}(\pm \pi/60)$
GM Pouring	CupA Pos	m	$\mathcal{U}(\pm 0.01)$
	CupA Rot	rad	$\mathcal{U}(\pm \pi/60)$
	CupB Pos	m	$\mathcal{U}(\pm 0.01)$
	CupB Rot	rad	$\mathcal{U}(\pm \pi/60)$
Drawer Opening	Handle Pos	m	$\mathcal{U}(\pm 0.01)$
Robot States	EEF Pos	m	$\mathcal{U}(\pm 0.01)$
	EEF Rot	rad	$\mathcal{U}(\pm \pi/60)$
	Joint Pos	rad	$\mathcal{U}(\pm \pi/60)$
Robot Controller	Gripper Velocity	m/s	$\mathcal{U}(\pm 0.005)$
	Gripper Delay	s	$\mathcal{U}(0.1, 0.3)$

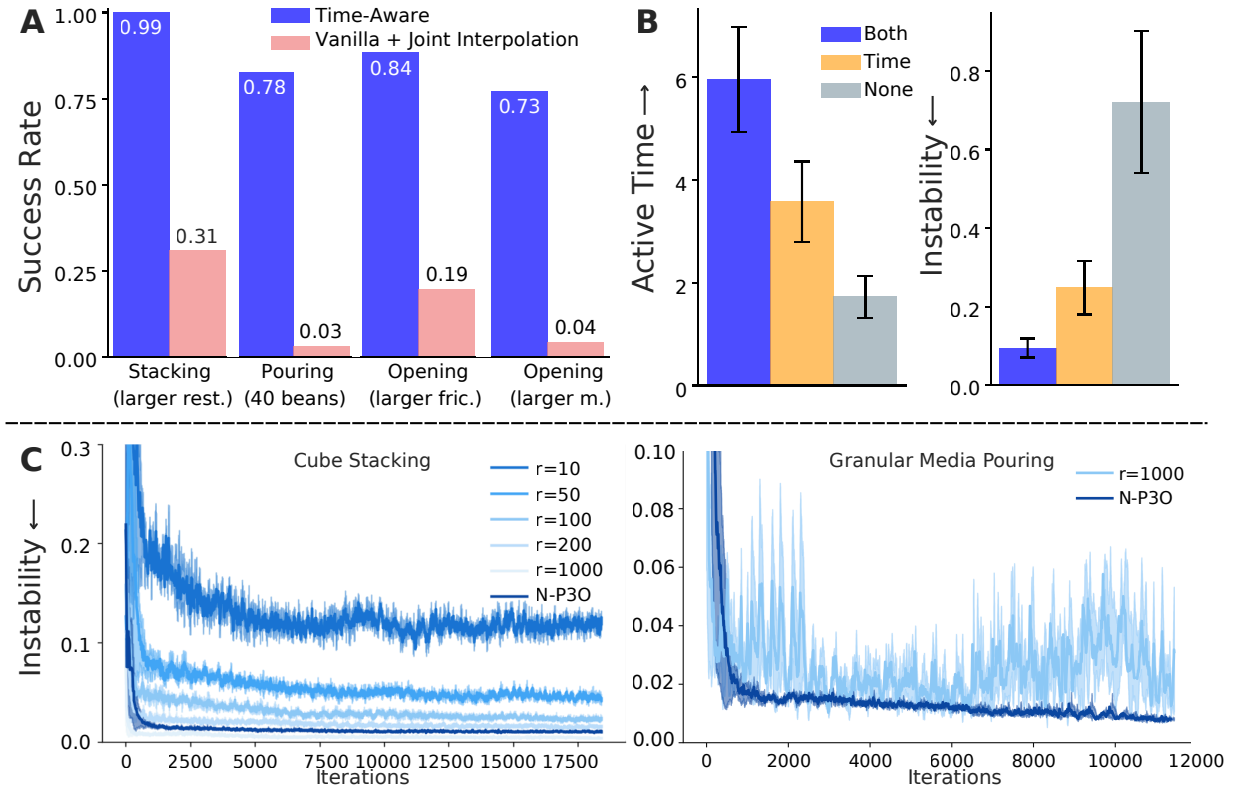


**Figure S1: Ablation studies and additional baselines.** (A) The vanilla policy with joint interpolation failed to adapt to environments requiring cautious behaviors, whereas the time-aware policy succeeded across all tasks despite these environmental variations being unseen during training. (B) The time objective increases active manipulation time and reduces instability. Explicitly combining stability and time objectives further improves time utilization and overall stability. (C) Without CMDP formulation, time-aware policy training becomes highly sensitive to reward scaling. For example, cube stacking requires sufficiently high instability reward scaling, but this same scaling destabilizes granular media pouring training entirely. In contrast, our CMDP-based approach generalizes across tasks and achieves stable performance without exhaustive reward tuning.

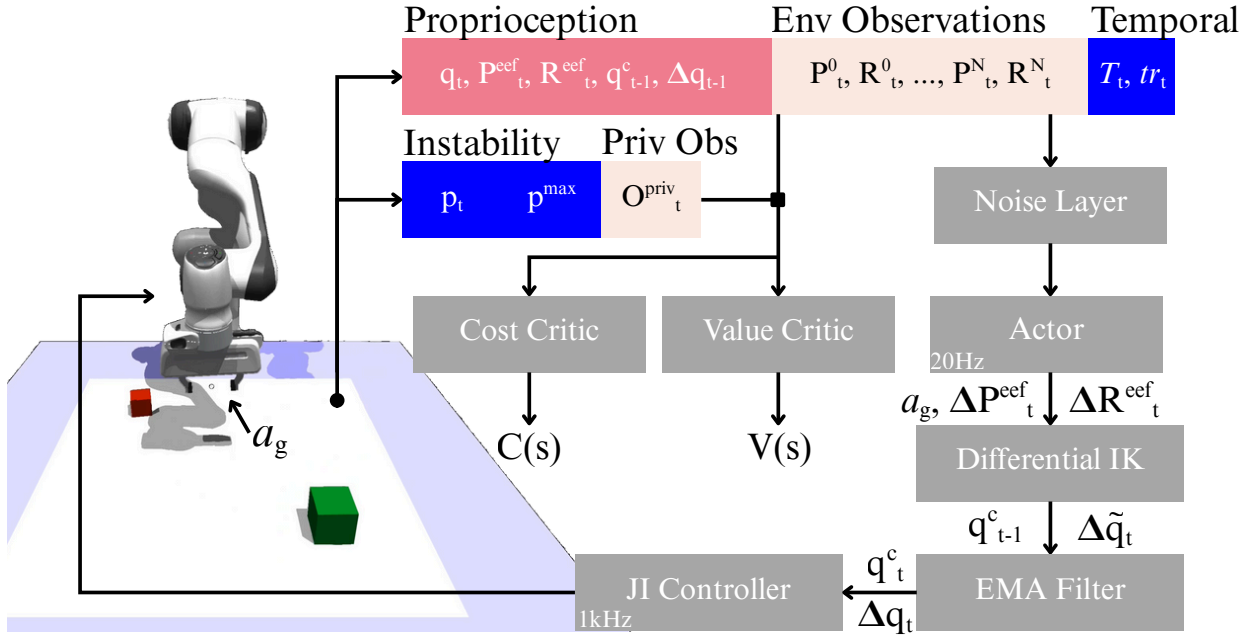


**Figure S2: Policy architecture and control loop.** During training, observations are passed through a noise layer before being input to the actor, which outputs 6-DoF end-effector relative poses and binary gripper actions at 20 Hz. These are converted to target joint positions via differential inverse kinematics, smoothed with an exponential moving average filter, and sent to the low-level joint impedance controller operating at 1 kHz. To address the challenge of measuring scene instability in real-world deployments, we employ an asymmetric actor–critic method. The critic observes noise-free observations and privileged information, while the actor uses only noisy and observable inputs. This design enables the actor to learn a deployable policy under partial observability while the critic leverages privileged information for accurate gradient shaping.

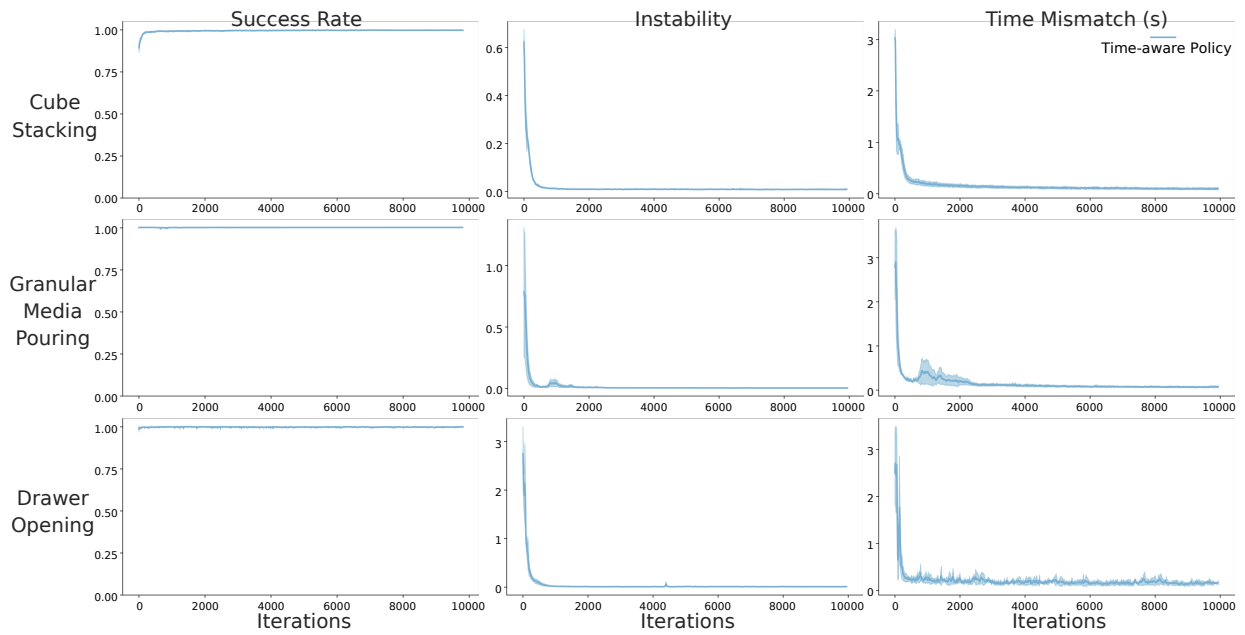


**Figure S3: Training curves of the time-aware policy.** Each experiment was conducted with five random seeds. The blue curve represents the mean across five training runs; the shaded region represents the standard deviation. The time-aware policy learning framework demonstrates strong training stability and convergence.